References

1 Bomman PC, Beckingham IJ. Pancreatic tumours. *Br Med J* 2001; **322**: 721–3.
2 Rosewicz S, Wiedenmann B. Pancreatic carcinoma. *Lancet* 1997; **349**: 485–9.
3 Sawabu N, Watanabe H, Yamaguchi Y, Ohtsubo K, Motoo Y. Serum tumor markers and molecular biological diagnosis in pancreatic cancer. *Pancreas* 2004; **28**: 263–7.
4 Kondo H, Sugano K, Fukayama N *et al.* Detection of point mutations in the K-ras oncogene at codon 12 in pure pancreatic juice for diagnosis of pancreatic carcinoma. *Cancer* 1994; **73**: 1589–94.
5 Furuya N, Kawa S, Akamatsu T, Furihata K. Long-term follow-up of patients with chronic pancreatitis and K-ras gene mutation detected in pancreatic juice. *Gastroenterology* 1997; **113**: 593–8.
6 Schena M, Shalon D, Davis RW, Brown PO. Quantitative monitoring of gene expression patterns with a complementary DNA microarray. *Science* 1995; **270**: 467–70.
7 Duggan DJ, Bittner M, Chen Y, Meltzer P, Trent JM. Expression profiling using cDNA microarrays. *Nat Genet* 1999; **21**: 10–4.
8 Yoshida K, Ueno S, Iwao T *et al.* Screening of genes specifically activated in the pancreatic juice ductal cells from the patients with pancreatic ductal carcinoma. *Cancer Sci* 2003; **94**: 263–70.
9 Terada T, Ohta T, Sasaki M, Nakamura Y, Kim YS. Expression of MUC apomucins in normal pancreas and pancreatic tumours. *J Pathol* 1996; **180**: 160–5.
10 Van Gelder RN, von Zastrow ME, Yool A, Dement WC, Barchas JD, Eberwine JH. Amplified RNA synthesized from limited quantities of heterogeneous cDNA. *Proc Natl Acad Sci USA* 1990; **87**: 1663–7.
11 Oshima Y, Ueda M, Yamashita Y *et al.* DNA microarray analysis of hematopoietic stem cell-like fractions from individuals with the M2 subtype of acute myeloid leukemia. *Leukemia* 2003; **17**: 1990–7.
12 Affymetrix [web site on the Internet]. Support: Mask files. Available from URL: http://www.affymetrix.com/support/technical/mask_files.affx
13 Golub TR, Slonim DK, Tamayo P *et al.* Molecular classification of cancer: class discovery and class prediction by gene expression monitoring. *Science* 1999; **286**: 531–7.
14 Broad Institute [web site on the Internet]. GeneCluster 2.0. Available from URL: http://www.broad.mit.edu/cancer/software/genecluster2/gc2.html
15 Fellenberg K, Hauser NC, Brors B, Neutzner A, Hoheisel JD, Vingron M. Correspondence analysis applied to microarray data. *Proc Natl Acad Sci USA* 2001; **98**: 10781–6.
16 ViSta. [web site on the Internet]. ViSta: the visual statistics system. Available from URL: http://www.visualstats.org
17 Alon U, Barkai N, Notterman DA *et al.* Broad patterns of gene expression revealed by clustering analysis of tumor and normal colon tissues probed by oligonucleotide arrays. *Proc Natl Acad Sci USA* 1999; **96**: 6745–50.
18 Dhanasekaran SM, Barrette TR, Ghosh D *et al.* Delineation of prognostic biomarkers in prostate cancer. *Nature* 2001; **412**: 822–6.
19 Shipp MA, Ross KN, Tamayo P *et al.* Diffuse large B-cell lymphoma outcome prediction by gene-expression profiling and supervised machine learning. *Nat Med* 2002; **8**: 68–74.
20 Dudoit S, Fridlyand J, Speed TP. [pre-print PDF on the Internet]. Comparison of discrimination methods for the classification of tumors using gene expression data. Available from URL: http://www.stat.berkeley.edu/tech-reports/index.html
21 Albig W, Kardalinou E, Drabent B, Zimmer A, Doenecke D. Isolation and characterization of two human H1 histone genes within clusters of core histone genes. *Genomics* 1991; **10**: 940–8.
22 Noto S, Maeda T, Hattori S, Inazawa J, Imamura M, Asaka M, Hatakeyama M. A novel human RasGAP-like gene that maps within the prostate cancer susceptibility locus at chromosome 1q25. *FEBS Lett* 1998; **441**: 127–31.
23 Nakaizumi A, Tatsuta M, Uehara H *et al.* Cytologic examination of pure pancreatic juice in the diagnosis of pancreatic carcinoma. The endoscopic retrograde intraductal catheter aspiration cytologic technique. *Cancer* 1992; **70**: 2610–4.
24 Strausberg RL, Feingold EA, Grouse LH *et al.* Generation and initial analysis of more than 15 000 full-length human and mouse cDNA sequences. *Proc Natl Acad Sci USA* 2002; **99**: 16 899–903.
25 Isaji S, Kawarada Y, Umemoto S. Classification of pancreatic cancer. Comparison of Japanese and UICC classifications. *Pancreas* 2004; **28**: 231–4.

Supplementary Material

The following supplementary material is available for this article online:

Table S1. Annotation information and expression intensity data for the genes shown in Figure 2A.

Table S2. Annotation information and expression intensity data for the genes shown in Figure 3B.

Genome-Wide Screening for Target Regions of Histone Deacetylases in Cardiomyocytes

Ruri Kaneda, Shuichi Ueno, Yoshihiro Yamashita, Young Lim Choi, Koji Koinuma, Shuji Takada, Tomoaki Wada, Kazuyuki Shimada, Hiroyuki Mano

Abstract—The acetylation status of core histones in cardiomyocytes has been linked to the development of cardiac hypertrophy and heart failure. Little is known, however, of the genes affected by abnormal histone acetylation in such pathological conditions. We recently developed a genome-wide screening method, differential chromatin scanning (DCS), to isolate genomic fragments associated with histones subject to differential acetylation. We have now applied DCS to H9C2 rat embryonic cardiomyocytes incubated with or without trichostatin A (TSA), a specific inhibitor of histone deacetylase (HDAC) activity. About 200 genomic fragments were readily isolated by DCS on the basis of the preferential acetylation of associated histones in TSA-treated cells. Quantitation of the amount of DNA in chromatin immunoprecipitates prepared with antibodies to acetylated histone H3 revealed that 37 of 38 randomly chosen DCS clones were preferentially precipitated from the TSA-treated cells, thus verifying the high fidelity of DCS. Epigenetic regulation of DCS clones was further confirmed in cells treated with sodium butyrate, another HDAC inhibitor, as well as in cardiac myocytes isolated from neonatal rats. The mRNA level of 9 (39%) of 23 genes corresponding to DCS clones changed in parallel with the level of histone acetylation in H9C2 cells. Furthermore, a physiological hypertrophic stimulus, cardiotrophin-1, affected the acetylation level of histones associated with genomic regions corresponding to certain DCS clones. Our data thus establish a genome-wide profile of HDAC targets in cardiomyocytes, which should provide a basis for further investigations into the role of epigenetic modification in cardiac disorders. (***Circ Res.* 2005;97:210-218.**)

Key Words: epigenetics ■ histone acetylation ■ trichostatin A ■ cardiomyocyte

Epigenetic modification of chromatin includes methylation of genomic DNA as well as acetylation, methylation, and phosphorylation of histone proteins. Such epigenetic changes play important roles in the regulation of gene transcriptional activity associated with cell growth and differentiation as well as with organ development.[1–3] Acetylation of core histones is mediated by histone acetyltransferases (HATs) and, in many instances, results in relaxation of chromatin structure and transcriptional activation of associated genes.[4] Histone deacetylases (HDACs) counteract HAT activity by catalyzing the removal of acetyl moieties from lysine residues in histone tails, thereby inducing chromatin condensation and transcriptional repression.[5]

Regulation of histone acetylation has been linked to cardiac hypertrophy. The HAT activity of CREB-binding protein (CBP) and p300 is thus required for the induction of hypertrophic changes in cardiac muscle cells by phenylephrine.[6] Consistent with this observation, inhibition of HDAC activity results in an increase in the size of muscle cells.[7] Furthermore, HDACs of class II (HDAC-4, -5, -7, and -9) suppress cardiac hypertrophy in part by binding to and inhibiting the activity of myocyte enhancer factor 2 (MEF2).[8] In contrast, however, HDAC2 together with Hop was found to promote cardiac hypertrophy in vivo in a manner sensitive to systemic administration of the HDAC inhibitor trichostatin A (TSA).[9] Moreover, HDAC inhibitors prevent hypertrophy and sarcomere organization in cultured cardiac myocytes,[10] suggestive of a positive role for HDACs in cardiac hypertrophy.

These seemingly discrepant findings may be attributable either to differential actions of different classes of HDACs (and, possibly, of HATs) with regard to myocyte hypertrophy or to a dissociation between the deacetylase activity of HDACs and a prohypertrophic function.[8] Clarification of the role of HATs and HDACs in hypertrophy would be facilitated by identification of the genes targeted by these enzymes during the induction of hypertrophic changes. Little is known, however, of the genes regulated by HATs or HDACs in myocytes. Induction of the atrial natriuretic peptide (ANP) gene is associated with acetylation of histones (H3 and H4) located in the 3′ untranslated region of the gene.[11] Histones bound to the β-myosin heavy chain gene have also been shown to be targeted by HATs in myocytes.[8]

Original received February 21, 2005; revision received June 1, 2005; accepted June 24, 2005.

From the Divisions of Functional Genomics (R.K., S.U., Y.Y., Y.L.C., K.K., S.T., T.W., H.M.) and Cardiovascular Medicine (R.K., S.U., K.S.), Jichi Medical School, Tochigi, Japan; and CREST (H.M.), Japan Science and Technology Agency, Saitama.

Correspondence to Dr Hiroyuki Mano, Division of Functional Genomics, Jichi Medical School, 3311-1 Yakushiji, Kawachigun, Tochigi 329-0498, Japan. E-mail hmano@jichi.ac.jp

Circulation Research is available at http://circres.ahajournals.org

DOI: 10.1161/01.RES.0000176028.18423.07

We have recently established a new technique, differential chromatin scanning (DCS),[12] for genome-wide screening of DNA regions associated with histones that are differentially acetylated between a given pair of cell or tissue samples. To isolate target genes of HDACs in cardiac myocytes, we have now applied DCS to a rat embryonic heart–derived myogenic cell line, H9C2, treated or not with TSA. More than 200 genomic fragments were readily isolated by DCS, and genomic regions corresponding to 37 clones of 38 examined were confirmed to be associated with differentially acetylated histones. Furthermore, the expression of genes located in or close to such regions paralleled the associated level of histone acetylation.

Materials and Methods

Cell Culture

H9C2 cells were obtained from American Type Culture Collection (Rockville, Md) and were maintained in Dulbecco's modified Eagle's medium (DMEM; Invitrogen) supplemented with 10% fetal bovine serum (Invitrogen) and 2 mmol/L L-glutamine. For preparation of the tester sample, cells were incubated for 24 hours with 300 nM TSA (Wako). For other treatments, cells were incubated with 2 or 4 mmol/L sodium butyrate (Sigma) for 24 hours or with 1 nM cardiotrophin-1 (Calbiochemy) for the indicated times.

Neonatal cardiac myocytes were prepared as described previously.[13] In brief, ventricular tissue was dissected from newborn rats and subjected to digestion overnight at 4°C with trypsin (1 mg/mL; Invitrogen) in Hanks' balanced salt solution (Invitrogen). Myocytes were harvested by subsequent digestion of the tissue with collagenase (Worthington,) and were centrifuged twice at 50*g* to remove less dense cells such as fibroblasts. Myocytes were then cultured in DMEM-F12 (Invitrogen) supplemented with 10% fetal bovine serum and 2 mmol/L L-glutamine.

Differential Chromatin Scanning

HDAC targets were screened in H9C2 cells by DCS as described previously.[12] In brief, both tester and driver cells were fixed and subjected to immunoprecipitation with antibodies to acetylated histone H3 with the use of a chromatin immunoprecipitation (ChIP) assay kit (Upstate Biotechnology). DNA fragments recovered from the immunoprecipitates were digested with *Rsa*I (New England Biolabs), and the digestion products were ligated to the TAG adapter (5′-CCACCGCCATCCGAGCCTTTCTGCCCGGG-3′/3′-GAAAGACGGGCCC-5′). After polymerase chain reaction (PCR)–mediated amplification with the TAG primer (5′-CCACCGCCATCCGAGCCTTTCTGC-3′), the tester and driver DNA samples were digested with *Xma*I and *Sma*I, respectively. The tester DNA (0.5 μg) was ligated to the first subtraction adapter (5′-GTGAGGGTCGGATCTGGCTGGCTC-3′/3′-CGACCGAGGGCC-5′), annealed with 40 μg of the driver DNA at 67°C for 20 to 24 hours, and then subjected to PCR with the first subtraction primer (5′-GTGAGGGTCGGATCTGGCTGGCTC-3′). After digestion of single-stranded DNA with mung-bean nuclease (New England Biolabs), the amplified products were subjected to digestion with *Xma*I followed by a second round of subtraction PCR with the second subtraction adapter (5′-GTTAGCGGACACAGGGCGGGTCAC-3′/3′-GCCCAGTGGGCC-5′) and second subtraction primer (5′-GTTAGCGGACACAGGGCGGGTCAC-3′). The final products were digested with *Xma*I and ligated into pBlueScript (Stratagene). *Escherichia coli* DH5α cell clones transformed with the resulting recombinant plasmids were grown in 96-well plates and subjected to direct plasmid purification in the plates with the use of a Montage Plasmid Miniprep$_{96}$ Kit (Millipore). The nucleotide sequences of the purified plasmids were then determined by Dragon Genomics Center (Mie) and were used to screen, with the BLAT search program,[14] the nucleotide sequence database (http://genome.ucsc.edu/) assembled in June 2003 by the Genome Bioinformatics Group of the University of California at Santa Cruz (UCSC).

Quantitation of DNA

Genomic fragments immunoprecipitated by antibodies to acetylated histone H3 (Upstate Biotechnology) were subjected to PCR with a QuantiTect SYBR Green PCR Kit (Qiagen). The amplification protocol comprised incubations at 94°C for 15 s, 60°C for 30 s, and 72°C for 1 minute. Incorporation of the SYBR green dye into PCR products was monitored in real time with an ABI PRISM 7700 sequence detection system (PE Applied Biosystems), thereby allowing determination of the threshold cycle (C_T) at which exponential amplification of PCR products begins. The C_T values for DNA molecules in the immunoprecipitates and for those in the original sample before immunoprecipitation were used to calculate the abundance of the former relative to that of the latter. The oligonucleotide primers for PCR were 5′-CCGGAAGAGGTGGTTATGTAAA-3′ and 5′-GCTAAGAAGGGACAGGGCTAAC-3′ for the H9C2T-2_D09 clone, 5′-GTTTGTCTGGAGCCTGTACTCTC-3′ and 5′-AAGTTCTCCGTTTCAGGATTCAC-3′ for the H9C2T-2_C06 clone, 5′-CACATCCTTGGTGCTTCTGA-3′ and 5′-GAGGAGGGTGAGGAGCTGAG-3′ for the H9C2T-1_E03-1 clone, and 5′-CCCGGTGTTCTGTACGTAGG-3′ and 5′-ACTGATGGAGCATCCACATTCT-3′ for the H9C2T-S-1-8 clone.

Quantitation of mRNA

Total RNA was prepared from the tester and driver cells with an RNeasy Mini column (Qiagen) and was subjected to reverse transcription (RT) with PowerScript reverse transcriptase (BD Biosciences Clontech) and an oligo(dT) primer. Portions of the resulting cDNA were subjected to PCR with a QuantiTect SYBR Green PCR Kit. The amplification protocol comprised incubations at 94°C for 15 s, 60°C for 30 s, and 72°C for 1 minute. The C_T values for cDNAs corresponding to glyceraldehyde-3-phosphate dehydrogenase (GAPDH) mRNA and the mRNAs of interest were used to calculate the abundance of the latter relative to that of the former. The C_T values for GAPDH mRNA determined with 10 μg of total RNA from TSA-treated or nontreated cells were 18.5±0.8 and 18.2±0.2 (mean±SD), respectively, validating the use of GAPDH mRNA as an internal control.

The oligonucleotide primers for PCR were 5′-AATGTATCCGTTGTGGATCTGAC-3′ and 5′-ATTGTCATACCAGGAAATGAGCTT-3′ for GAPDH, 5′-GCCTGTGATACTCTGCTTATGTGT-3′ and 5′-CTTGAGGATTTCCTCTTTCTTCTG-3′ for the inositol 1,4,5-trisphosphate receptor type 3 gene (Itpr3), 5′-CAGTACCCTGTTGAGTCATCTCTG-3′ and 5′-GAAAGCAAGGTCTTCTTATTCTGG-3′ for the NAD(P)H dehydrogenase, quinone 1 gene (Nqo1), 5′-GCCTTCTACCTGCATACTACCAAG-3′ and 5′-AGTCTCAAGATACCGGAGCACA-3′ for the metastasis-associated 1 gene (Mta1), and 5′-CTGTTGGTACCTGTGCTGTGTAG-3′ and 5′-ACTGGTAGAGTACGTCCTTGTGG-3′ for the Jagged2 precursor gene (Jag2).

Statistical Analysis

Quantitation of DNA or mRNA was performed in triplicate in at least 2 independent experiments, and data are presented as mean±SD. The statistical significance of differences was analyzed by Student *t* test, with a probability value of <0.05 being considered significant.

Results

DCS in H9C2 Cells

Given that the ANP gene is a known target of HDAC in myocytes,[11] we first examined the effect of TSA on the acetylation level of histones bound to this gene in H9C2 cells. Real-time PCR analysis revealed that the amount of the 3′ untranslated region of the ANP gene that was precipitated by antibodies to acetylated histone H3 from TSA-treated cells was 7.85 times that precipitated from nontreated cells (data

not shown), indicating that the ANP gene is indeed a target of HDAC activity in H9C2 cells.

With the use of TSA-treated cells as the tester and nontreated cells as the driver, we then performed DCS, which in effect couples ChIP with subtraction PCR. After the second round of subtraction PCR, we sequenced the isolated genomic clones in a 96-well plate format. Analysis of 3 such plates thus yielded the nucleotide sequences of 288 DCS products. Among these randomly selected products, 222 clones contained >50 bp and were used to screen the nucleotide sequence database of UCSC with the use of the BLAT program.

A total of 195 clones showed >95% sequence identity to the rat genome sequence, and 178 of these clones were located either within protein-coding genes (demonstrated or predicted) or in the vicinity (within 10 kbp) of such genes (119 independent genes) (Table 1; Table SI available in the online supplement at http://circres.ahajournals.org). Forty-two (23.6%) of the 178 clones were assigned to a region spanning the promoter (0 to −2000 bp relative to the transcriptional start site), the first exon, and the first intron of the corresponding genes. Given that protein-coding genes account for only a few percent of the rat genome,[15] our data suggest that histone acetylation occurs preferentially at regions of the genome involved directly in transcriptional regulation.

Eleven DCS clones were assigned to overlapping sequences upstream of the Oct11 gene, and 7 clones were mapped to overlapping sequences at chromosomal position 8q24, a region with no annotation information (data not shown). The isolation of such multiple clones for individual genomic regions suggests that the DCS products isolated may represent most HDAC targets in H9C2 cells.

HDAC Targets in a Cardiomyocyte Cell Line

To verify the fidelity of DCS, we randomly selected 38 DCS clones and quantified the corresponding genomic fragments in immunoprecipitates prepared from both tester and driver cells with antibodies to acetylated histone H3. The amount of each DNA fragment in the immunoprecipitate relative to that in the original sample before ChIP was determined by real-time PCR. Selective amplification by DCS proved to be highly reliable (Table 1), with 37 of the 38 clones exhibiting tester-selective precipitation (tester/driver ratio of ≥1.5). It is therefore likely that DCS indeed identified targets of HDAC in myocytes.

To visualize directly the genome-wide distribution of HDAC targets, we mapped to rat chromosome figure our genomic clones whose chromosomal positions were known (Figure 1). The HDAC targets were distributed widely throughout the rat genome, although some "hot spots" for deacetylation were apparent. For example, 7 of the DCS clones mapped to chromosomal position 5q36, and detailed mapping revealed that all of these clones were located within a region spanning 27 Mbp. It is thus possible that regional alterations of chromatin structure result in coordinated transcriptional regulation of genes within the affected region.

Some of the clones listed in Table 1 correspond to loci within or close to rat genes whose products function in intracellular calcium mobilization or antioxidant processes. One such clone (H9C2T-2_D09), for instance, mapped to a region encompassing intron 21 and exon 22 of Itpr3 (Figure 2A), which encodes a receptor for inositol 1,4,5-trisphosphate that plays an important role in Ca^{2+}-mediated signal transduction. The cytosolic concentration of Ca^{2+} directly regulates muscle contraction and cardiac rhythm and is a determinant of myocyte hypertrophy and heart failure.[16] The amount of the genomic fragment corresponding to the H9C2T-2_D09 clone was 6.6-fold greater in the ChIP product of TSA-treated cells than in that of untreated cells (Figure 2B), indicating that the extent of histone acetylation in this region of the genome of the tester cells was 6.6 times that in the driver cells. Furthermore, inhibition of HDAC activity was accompanied by an increase in the amount of Itpr3 mRNA (Figure 2C). These data suggest that HDAC actively deacetylates a chromosomal region corresponding to Itpr3 and thereby suppresses the transcriptional activity of the gene.

Another clone (H9C2T-2_C06) was mapped to the first intron of Nqo1 (Figure 2D), which encodes a reductase that contributes to detoxification of quinones and to regulation of apoptosis.[17] We examined whether the acetylation of associated histones and the expression of Nqo1 are regulated by HDAC activity in cardiomyocytes. As with Itpr3, the acetylation level of histones bound to Nqo1 was increased by TSA treatment in H9C2 cells (Figure 2E), and this epigenetic change was accompanied by an increase in the amount of Nqo1 mRNA (Figure 2F).

Nineteen (10.7%) of the 178 clones whose chromosomal location was known were assigned to loci corresponding to at least 2 genes in the rat genome. One such clone, H9C2T-1_E03-1, was mapped to a region corresponding to the first intron of Mta1 and to the last exon of Jag2 (Figure 3A). Histone acetylation in this region might thus affect the transcription of both genes simultaneously. The level of histone H3 acetylation in this region was confirmed to be greater in the tester cells than in the driver cells (Figure 3B). However, although inhibition of HDAC activity by TSA resulted in upregulation of the amount of Jag2 mRNA (Figure 3C), it had no effect on the abundance of Mta1 mRNA (Figure 3D). Histone acetylation in the genomic region that encompasses both Jag2 and Mta1 thus appears to regulate the transcriptional activity of the former gene but not that of the latter. Jag2 is a ligand for the receptor Notch1 and is abundant in the heart.[18] Coculture of fibroblasts expressing human JAG2 with murine C2C12 myoblasts resulted in inhibition of myogenic differentiation of the latter cells, implicating JAG2 in regulation of this process.

We selected an additional 19 DCS clones for quantitation of the corresponding mRNAs. Among the genes examined, 6 were preferentially expressed (tester/driver ratio of ≥1.5) in the TSA-treated cells compared with the nontreated cells (Table 1).

Regulation of Histone Acetylation in Neonatal Rat Cardiac Myocytes

Our DCS analysis identified HDAC targets in a cardiomyocyte cell line. To investigate whether the level of histone

Fragments of the Rat Genome Isolated by DCS in H9C2 Cells

Clone ID	Tester/Driver DNA Ratio	Annotation	GenBank Accession No. (or Ensemble Gene ID)	Locus	Tester/Driver mRNA Ratio	Position Relative to Corresponding Genes
H9C2T-S-2–8	13.7	EST	BQ204614	19q12	5.34	Intron 2
H9C2T-S-1-5b	10.92	Skn-1a	L23862	8q22		4 kbp upstream of exon 1
H9C2T-1_D09	10.7	Putative G protein–coupled receptor (SENR) gene (Senr)	NM_020537	10q32.3	1.09×10^6	Exon 1
H9C2T-S-1-2b	9.36	NA	NA	20p12		
H9C2T-1_B05	8.43	No description	(ENSRNOG00000013959)	8q24		Last exon+last intron
H9C2T-S-1-8	7.96	Myocilin (Myoc)	NM_030865	13q22	2.03	2.5 kbp upstream of exon 1
H9C2T-1_E03-1*	7.85	Mta1 (mta1)	NM_022588	6q32	0.91	Intron 1
		Jagged2 precursor	U70050		8.43	Last exon
H9C2T-2_E05	7.7	Protein kinase C and casein kinase substrate in neurons 1 (Pacsin1)	NM_017294	20p12	26.45	Intron 1
H9C2T-1_C04-2	7.69	Carbohydrate (chondroitin 6/keratan) sulfotransferase 3 (Chst3)	NM_053408	20q11	0.25	Intron 1
H9C2T-S-1-2a	6.99	Phosphodiesterase	L27061	16p14	1.12×10^8	1.3 kbp upstream of exon 1
H9C2T-S-1-4	6.76	EST	CB741111	14p22		Intron 3
H9C2T-S-1-5a	6.64	Brain and reproductive organ–expressed protein	NM_199270	6q13		Intron 10
H9C2T-1_C04-1	6.61	EST	CO562897	3q43		Exon 1
H9C2T-2_D09	6.6	Inositol 1,4,5-trisphosphate receptor 3 (Itpr3)	NM_013138	20p12	1.66	Intron 21+exon 22
H9C2T-2_E11	6.51	EST	CV077786	3q43		Last exon
H9C2T-1_H05-1	6.29	Microtubule-associated protein tau (Mapt)	NM_017212	10q32.1	602.17	Intron 7
H9C2T-1_G12	5.83	No description	(ENSRNOG00000004217)	10q12		Intron 2
H9C2T-1_H01	5.36	A disintegrin and metalloproteinase domain 1 (fertilin alpha) (Adam1)	NM_020078	12q16	0.46	Last intron
H9C2T-2_F10-1	5.13	Translocase of outer mitochondrial membrane 20 homolog (yeast) (Tomm20)	NM_152935	19q12		Last intron
H9C2T-S-1-7	5.06	EST	BF282351	4q34	0.68	2 kbp upstream of exon 1
H9C2T-1_H10	4.92	Collagen, type V, alpha 1 (Col5a1)	NM_134452	3p12	0.86	Intron 1
H9C2T-2_H07	4.4	Runt-related transcription factor 1 (Runx1)	NM_017325	11q11	1.21	Intron 4
H9C2T-S-1-3	4.36	No description	(ENSRNOG00000021887)	8q32		Last exon+last intron
H9C2T-S-2-3	4.35	EST	CO557128	1q43		0.5 kbp upstream of exon 1
H9C2T-2_A01'	3.9	Fos-like antigen 1 (Fosl1)	NM_012953	1q43	0.39	1 kbp downstream of last exon
H9C2T-S-2-7	3.86	Arylsulfatase B (ARSB)	D49434	2q12	0.48	Intron 4
H9C2T-1_F10	3.85	Phosphatidylinositol 4-kinase (Pik4cb)	NM_031083	2q34	0.88	Exon 4
H9C2T-2_C06	3.78	NAD(P)H dehydrogenase, quinone 1 (Nqo1)	NM_017000	19q12	2.82	Intron 1
H9C2T-1_D03	3.79	Cytokine-inducible SH2-containing protein	AF065161	8q32	1.47	Last exon
H9C2T-1_F09-1*	3.74	EST	CK597511	15p16		Immediately upstream of exon 1
		Normalized rat muscle, Bento Soares Rattus sp. cDNA clone RMUBG18 3' end	AI171102			Intron 1
		EST	CK598708			Exon 1
H9C2T-2_B07	3.62	Cyclin D1 (Ccnd1)	NM_171992	1q42	0.59	Intron 3+exon 4
H9C2T-1_C03-1	3.58	G protein beta subunit–like (Gbl)	NM_022404	10q12	0.77	Last exon
H9C2T-2_A11	3.4	EST	CO557128	1q43		0.5 kbp upstream of exon 1
H9C2T-S-2-1	3.37	Period1 (rper1), partial cds	AB092976	10q24	0.52	Introns 15, 16+exon 16
H9C2T-2_E03-2	2.94	Interleukin-11 (Il11)	NM_133519	1q12	1	Intron 5
H9C2T-S-1-1	2.69	No description	(ENSRNOG00000001730)	11q22		Intron 3
H9C2T-1_C09	1.83	No description	(ENSRNOG00000025448)	10q32.1		0.5 kbp upstream of exon 1

EST indicates expressed sequence tag; NA, not assigned. *Fragments that mapped to loci of multiple genes.

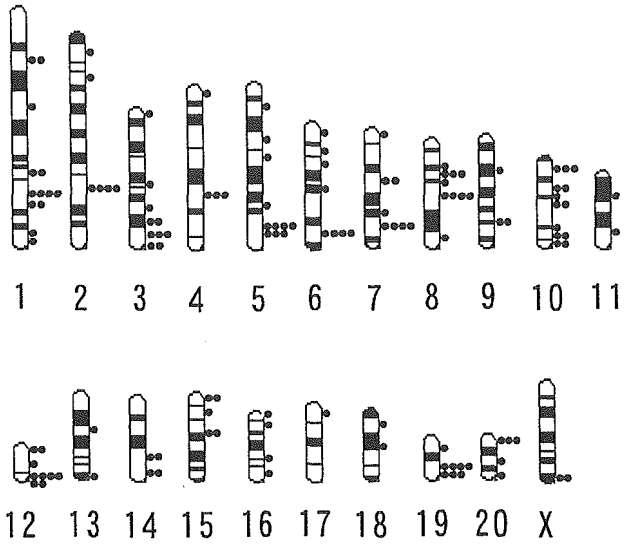

Figure 1. Chromosomal distribution of HDAC targets in rat cardiomyocytes. Genomic fragments (red dots) isolated by DCS were mapped to rat chromosomes.

acetylation at these targets is also affected by HDAC activity in differentiated cardiomyocytes, we isolated cardiac myocytes from neonatal rats and incubated these cells in the absence or presence of TSA. Consistent with the results obtained with H9C2 cells (Figures 2 and 3), TSA treatment resulted in marked increases both in the acetylation level of histones associated with the genomic locus corresponding to clone H9C2T-2_D09 and in the amount of Itpr3 mRNA in neonatal rat cardiac myocytes (Figure 4A). Similarly, TSA increased both the histone acetylation level for genomic DNA corresponding to clone H9C2T-2_C06 and the abundance of Nqo1 mRNA in the rat cardiac myocytes (Figure 4B). Furthermore, TSA increased the level of histone acetylation associated with the genomic locus corresponding to clone H9C2T-1_E03-1 in rat cardiac myocytes and, as in H9C2 cells, it increased the amount of Jag2 mRNA without affecting that of Mta1 mRNA (Figure 4C). Quantitation of genomic DNA corresponding to an additional 19 DCS clones in ChIP products prepared from neonatal rat cardiac myocytes revealed that the acetylation level of bound histones was increased by a factor of >5 by TSA treatment (data not shown). These data thus indicate that the genomic clones identified by DCS in H9C2 cells represent genomic regions whose associated histones are targeted by HDAC activity in differentiated cardiac myocytes. Twelve of the 23 genes that mapped to (or in the vicinity of) the DCS clones examined were also transcriptionally activated by a factor of >1.5 in the TSA-treated neonatal rat cardiac myocytes compared with nontreated cells (data not shown).

Effects of Sodium Butyrate on Histone Acetylation

Various compounds other than TSA inhibit HDAC activity with different target preferences.[19] Sodium butyrate, for example, inhibits the catalytic activity of HDACs belonging to class I or IIA, whereas TSA inhibits that of HDACs belonging to class I, IIA, or IIB. We therefore examined

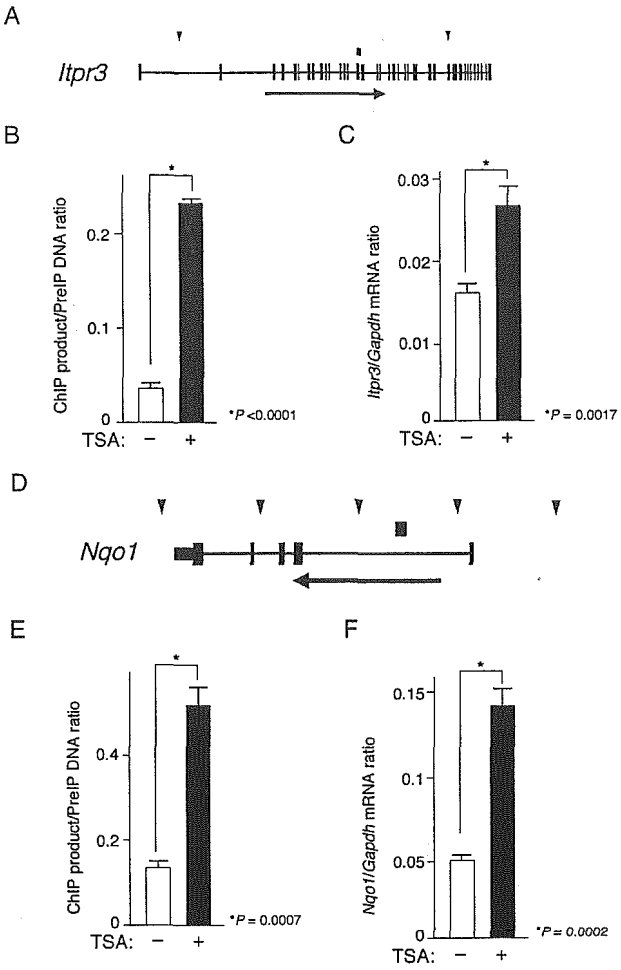

Figure 2. Identification of Itpr3 and Nqo1 as targets of HDAC in cardiomyocytes. A, One of the DCS clones (H9C2T-2_D09; red rectangle) was mapped to chromosome 20p12, spanning intron 21 and exon 22 of Itpr3. Exons are denoted by black boxes, the arrow indicates the direction of transcription, and blue triangles depict distance markers separated by 50 kbp. B, Chromatin immunoprecipitates were prepared from H9C2 cells treated (+) or not (−) with 300 nM TSA for 24 hours. The amount of DNA corresponding to the H9C2T-2_D09 sequence in each ChIP product relative to that in the corresponding original sample before immunoprecipitation (PreIP) was then determined by real-time PCR. C, The amount of Itpr3 mRNA relative to that of GAPDH mRNA in H9C2 cells treated or not with TSA was determined by quantitative RT-PCR. D, One of the DCS clones (H9C2T-2_C06; red rectangle) was mapped to chromosome 19q12 in the first intron of Nqo1. Green triangles depict distance markers separated by 5 kbp. E, The amount of genomic DNA corresponding to the H9C2T-2_C06 sequence in ChIP products relative to that in the PreIP samples was measured as in B. F, The amount of Nqo1 mRNA relative to that of GAPDH mRNA was determined as in C. All data are mean±SD of triplicates from representative experiments that were performed at least twice. Probability values for the indicated comparisons were determined by Student *t* test.

whether sodium butyrate also affects the acetylation level of histones associated with our DCS clones.

H9C2 cells or neonatal rat cardiac myocytes were incubated for 24 hours with 0, 2, or 4 mmol/L sodium butyrate and then subjected to ChIP, and the resulting products were subjected to real-time PCR to quantitate the amount of genomic DNA corresponding to the clones

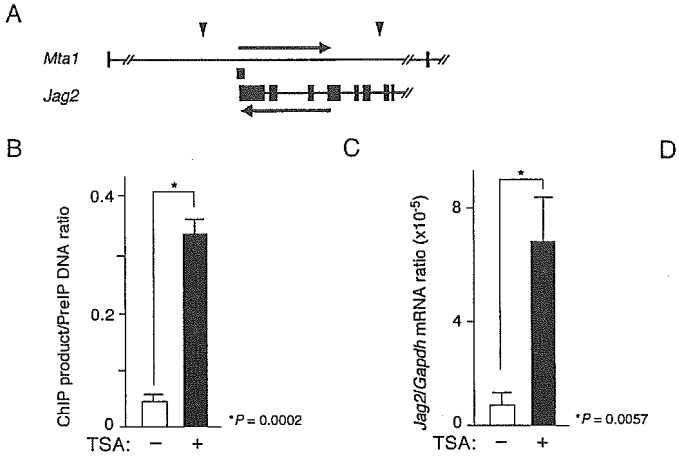

Figure 3. Identification of Mta1 and Jag2 as targets of HDAC in cardiomyocytes. A, One of the DCS clones (H9C2T-1_E03-1; red rectangle) was mapped to chromosome 6q32 in the first intron of Mta1 and the last exon of Jag2. The position of the H9C2T-1_E03-1 clone in the genome is shown schematically as in Figure 2D. B, The amount of genomic DNA corresponding to the H9C2T-1_E03-1 sequence in ChIP products relative to that in the PreIP samples was measured by real-time PCR as in Figure 2B. C and D, The amounts of Jag2 (C) and Mta1 (D) mRNAs relative to that of GAPDH mRNA were determined as in Figure 2C. All data are mean±SD of triplicates from representative experiments, and probability values for the indicated comparisons were determined by Student *t* test.

H9C2T-2_D09, H9C2T-2_C06, or H9C2T-1_E03-1. Treatment with sodium butyrate at either 2 or 4 mmol/L resulted in marked increases in the amount of DNA corresponding to each clone in the ChIP products from both H9C2 cells (Figure 5A) and neonatal rat cardiac myocytes (Figure 5B). Although the magnitudes of the effects of 2 and 4 mmol/L sodium butyrate were similar in H9C2 cells, the effects of the higher concentration were greater than those of the lower concentration in the differentiated cardiac myocytes. The genomic regions corresponding to these 3 DCS clones were thus epigenetically regulated by both TSA and sodium butyrate.

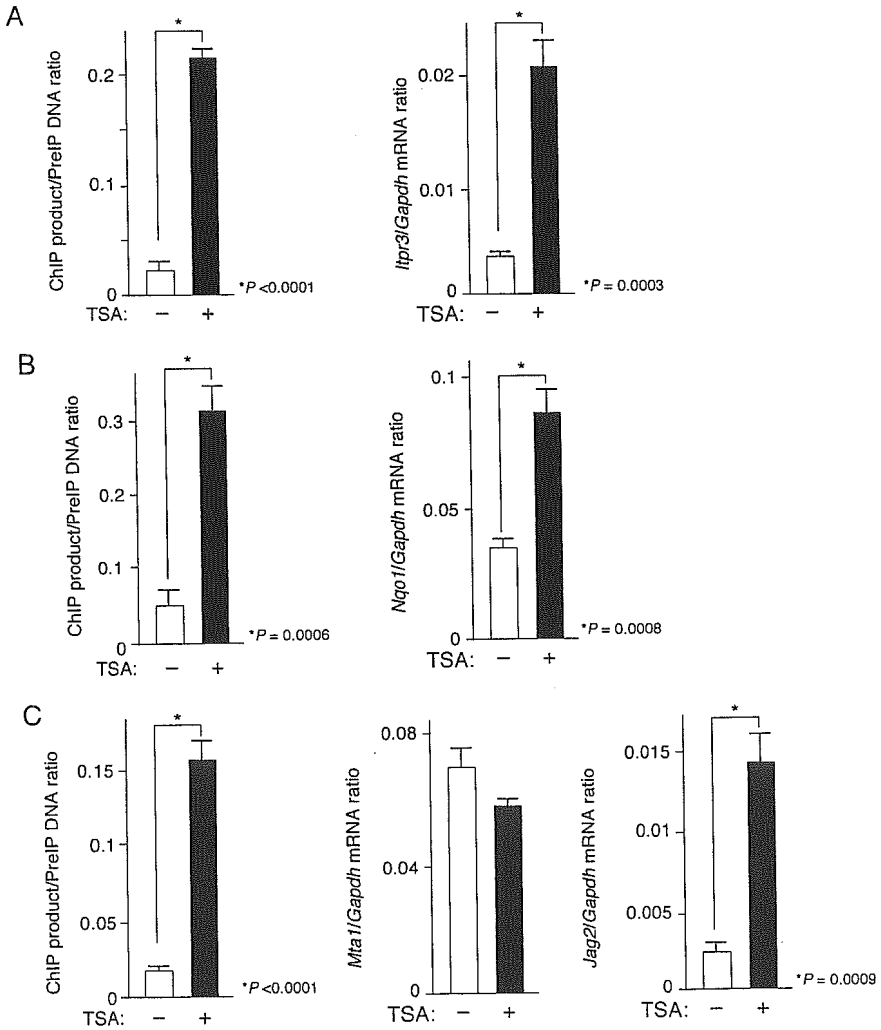

Figure 4. Histone acetylation status and gene expression in neonatal rat cardiac myocytes. Chromatin immunoprecipitates were prepared from freshly isolated cardiac myocytes treated (+) or not (−) with 300 nM TSA for 24 hours, and the amount of DNA corresponding to the H9C2T-2_D09 (A), H9C2T-2_C06 (B), or H9C2T-1_E03-1 (C) clones in each ChIP product was determined by real-time PCR. The amount of Itpr3 (A), Nqo1 (B), or Mta1 and Jag2 (C) mRNAs in cells treated or not with TSA was determined by quantitative RT-PCR. All data are mean±SD of triplicates from representative experiments, and probability values for the indicated comparisons were determined by Student *t* test.

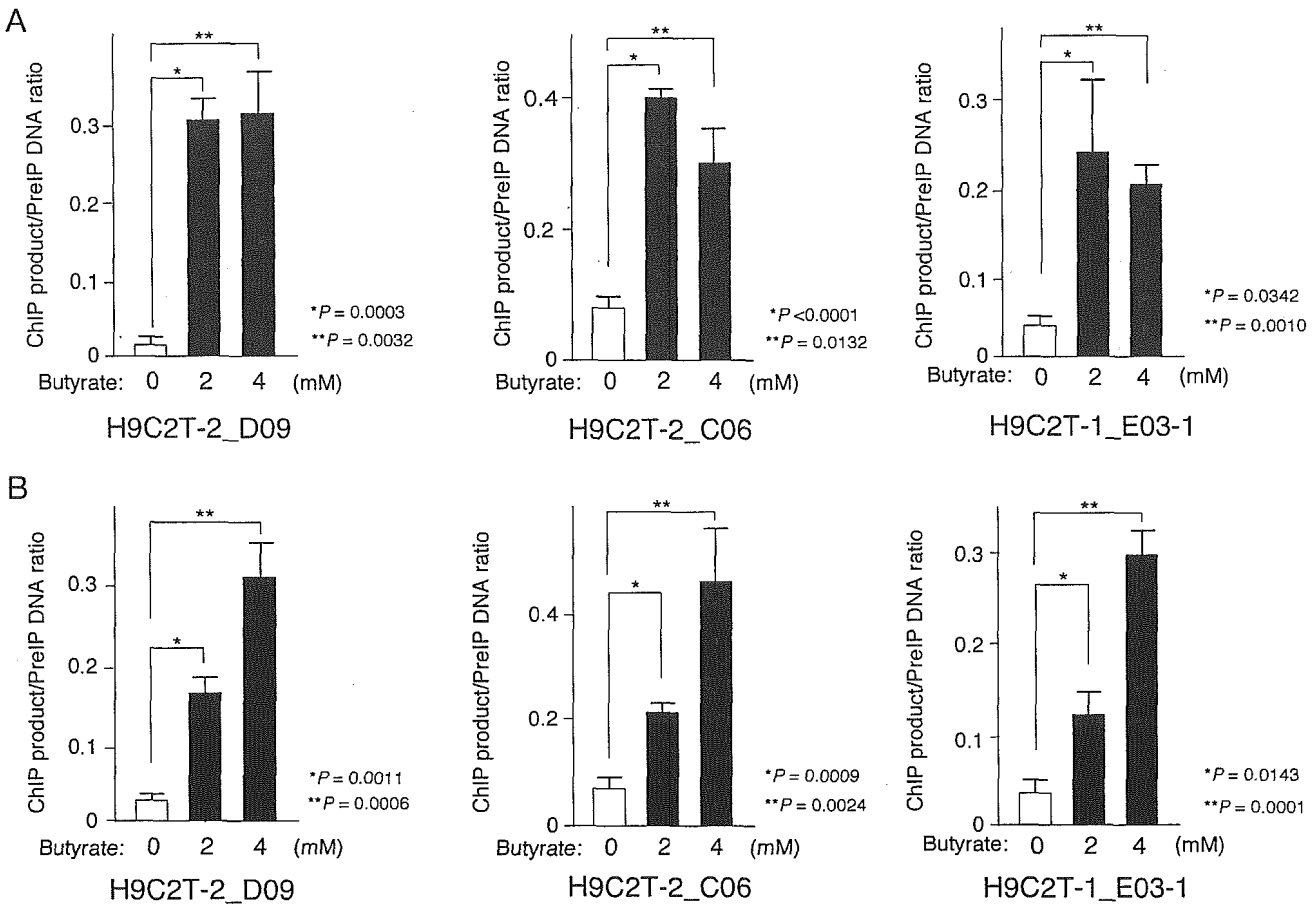

Figure 5. Regulation of histone acetylation status by sodium butyrate. Chromatin immunoprecipitates were prepared from H9C2 cells (A) or freshly isolated rat neonatal cardiac myocytes (B) after treatment with 0, 2, or 4 mmol/L sodium butyrate for 24 hours, and the amount of DNA corresponding to the H9C2T-2_D09, H9C2T-2_C06, or H9C2T-1_E03-1 clones in each ChIP product was determined. All data are mean±SD of triplicates from representative experiments, and probability values for the indicated comparisons were determined by Student *t* test.

Regulation of HDAC Targets by a Hypertrophic Stimulus

Given that H9C2 cells retain the ability to undergo hypertrophic changes in response to various stimuli,[20,21] we next examined whether stimulation with a physiological hypertrophic agent, cardiotrophin-1 (CT-1), affects the extent of histone acetylation at genomic regions corresponding to DCS clones in these cells. H9C2 cells were incubated with 1 nM CT-1 for various times up to 24 hours and were then subjected to ChIP and real-time PCR analysis. Quantitation of genomic DNA revealed that the level of histone acetylation at the region corresponding to clone H9C2T-1_E03-1 was increased significantly at 6 hours and was still increasing at 24 hours (Figure 6A). Similar to the effects of TSA at this locus (Figure 3), the increase in histone acetylation induced by CT-1 was not accompanied by a change in the amount of Mta1 mRNA (Figure 6B), but was associated with a transient activation of Jag2 transcription apparent after stimulation for 6 hours (Figure 6C).

Finally, we analyzed a different DCS clone for epigenetic regulation by CT-1. The H9C2T-S-1-8 clone corresponds to the promoter region for the Myocilin (Myoc) gene (Figure 6D). This gene encodes a protein involved in cytoskeletal function, and mutations in Myoc have been shown to cause a hereditary form of juvenile-onset open-angle glaucoma.[22] We found that CT-1 induced a time-dependent increase in the extent of histone acetylation at the genomic region corresponding to this DCS clone (Figure 6E). Together, these data indicate that the histone acetylation level of genomic regions corresponding to our DCS clones is regulated not only by TSA and sodium butyrate but also by physiological stimuli.

Discussion

With the use of our recently developed screening method, DCS, we have now identified almost 200 HDAC targets in cardiomyocytes. The acetylation of histones associated with genomic regions corresponding to 37 of 38 randomly chosen DCS clones was confirmed to be induced by treatment of H9C2 cells with TSA. Genomic regions corresponding to DCS clones were also epigenetically regulated by another HDAC inhibitor, sodium butyrate. Furthermore, the histone acetylation level of genomic regions corresponding to all 22 DCS clones examined was shown to be HDAC targets also in freshly isolated cardiac myocytes. Finally, the acetylation level of histones associated with DCS clones was shown to be regulated by a physiological stimulus, CT-1. The genomic

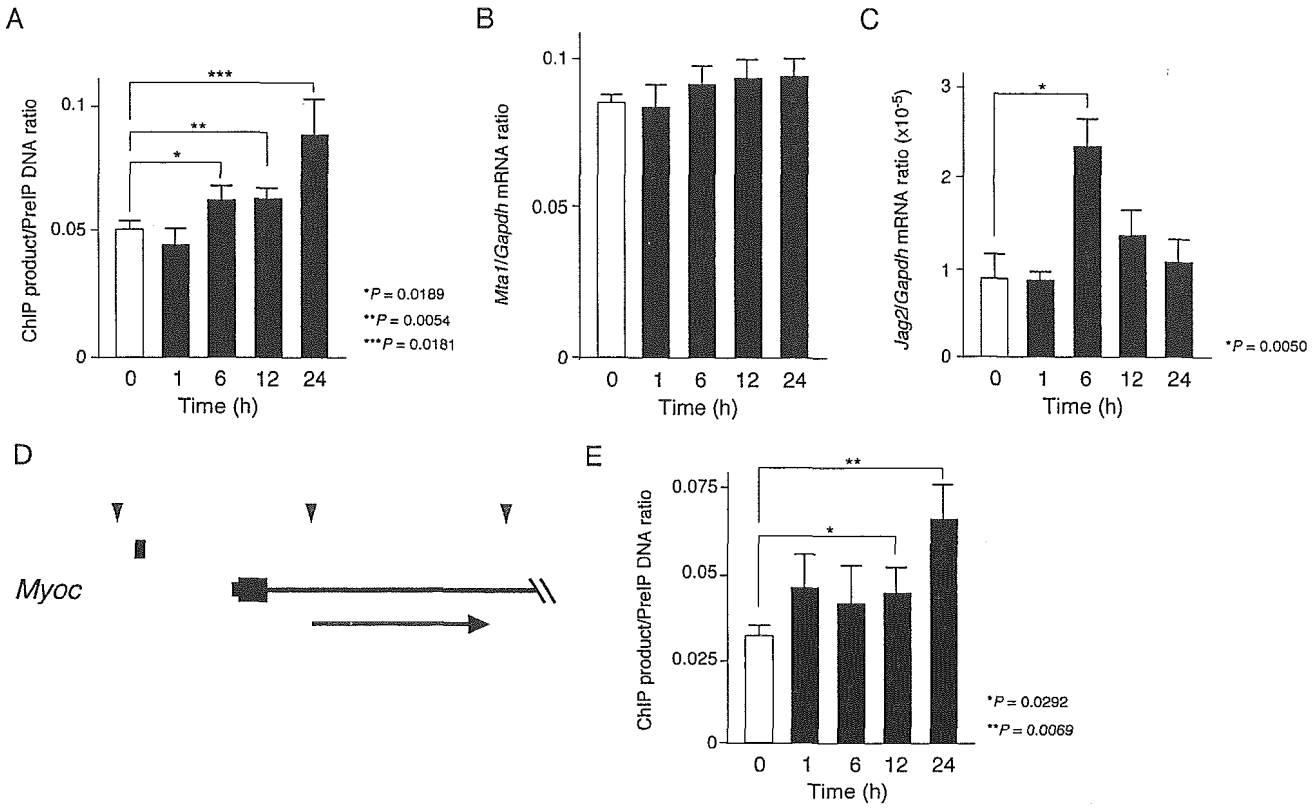

Figure 6. Effects of CT-1 on histone acetylation in H9C2 cells. A, H9C2 cells stimulated with CT-1 (1 nM) for the indicated times were subjected to ChIP, and the amount of genomic DNA corresponding to the DCS clone H9C2T-1_E03-1 was determined in ChIP products. B and C, The amounts of Mta1 (B) and Jag2 (C) mRNAs relative to that of GAPDH mRNA were determined by quantitative RT-PCR in H9C2 cells stimulated with CT-1 for the indicated times. D, The H9C2T-S-1-8 clone (red rectangle) was mapped to chromosome 13q22 in the promoter region of Myoc. The position of the clone in the genome is shown schematically as in Figure 2D. E, The amount of genomic DNA corresponding to the H9C2T-S-1-8 sequence was determined in ChIP products prepared from H9C2 cells treated with CT-1 for the indicated times. All data are mean±SD of triplicates from representative experiments, and probability values for the indicated comparisons were determined by Student *t* test.

loci identified by DCS thus include physiologically relevant targets for epigenetic modification.

The HDAC targets identified in cardiomyocytes include several genes related to cell growth or differentiation that might play an important role in heart function. In addition to Itpr3 and Jag2, such genes include those for G protein–coupled receptors (Senr, Gbl), regulators of cytosolic Ca^{2+} concentration (phosphodiesterase, Pik4cb, Pacsin1), and mediators of growth signaling (Ccnd1, Runx1, Fosl1, Il11, Oct11, Sox6) (online Table SI). Our data suggest that these various genes are under epigenetic control in cardiomyocytes, a conclusion that was verified for some of them by the demonstration that the level of acetylation of associated histones was regulated by the physiological stimulus CT-1. Although CT-1 has not previously been shown to elicit intracellular signaling that affects histone acetylation, our data now indicate that this is indeed the case.

Many (42 of 178) of our DCS clones mapped to the 5′-regions of genes in the rat genome. Bernstein et al recently attempted to identify loci in the human genome whose associated histones are acetylated.[23] These researchers used the "ChIP on chip"[24] strategy with high-density genome-tilling microarrays for human chromosomes 21 and 22. Interestingly, consistent with our results, they found that histone H3 acetylated on lysine-9 and lysine-14 was preferentially localized at the 5′ ends of genes, with 58% of such sites of histone acetylation residing in regions encompassing −1.0 to +1.0 kbp of known genes.

Acetylation of core histones is not always associated with the regulation of gene transcription, however. Histone acetylation may thus be related to chromosome replication or to chromatin remodeling unrelated to transcriptional regulation.[25] In addition, various types of covalent modification, including acetylation, phosphorylation, and methylation, may exert their effects on histones in a coordinated manner, resulting in the generation of a so-called histone code.[26] Consistent with these considerations, only 39% and 52% of the genes corresponding to DCS clones examined showed preferential expression in TSA-treated H9C2 cells and TSA-treated neonatal rat cardiac myocytes, respectively, compared with the corresponding untreated cells.

Although DCS does not readily allow a quantitative comparison of the level of histone acetylation between samples, our method is technically straightforward and does not require any specialized apparatus such as a DNA microarray system. In conclusion, DCS enabled us to efficiently identify HDAC targets in cardiomyocytes. Our present data support the feasibility of determining genome-wide histone acetyla-

tion profiles of the cardiovascular system. They should also provide a basis for further characterization of the importance of epigenetic alterations in the development of cardiac hypertrophy or heart failure. Application of DCS to human heart specimens has the potential to highlight such information of clinical relevance.

Acknowledgments

This work was supported in part by a Grant-in-Aid for Scientific Research on Priority Areas (C) "Medical Genome Science" from the Ministry of Education, Culture, Sports, Science, and Technology of Japan and by a grant from Salt Science Research Foundation (#04C7).

References

1. Baylin SB, Herman JG. DNA hypermethylation in tumorigenesis: epigenetics joins genetics. *Trends Genet.* 2000;16:168–174.
2. van Leeuwen F, Gottschling DE. Genome-wide histone modifications: gaining specificity by preventing promiscuity. *Curr Opin Cell Biol.* 2002; 14:756–762.
3. Burgess-Beusse B, Farrell C, Gaszner M, Litt M, Mutskov V, Recillas-Targa F, Simpson M, West A, Felsenfeld G The insulation of genes from external enhancers and silencing chromatin. *Proc Natl Acad Sci U S A.* 2002;99:16433–16437.
4. Carrozza MJ, Utley RT, Workman JL, Cote J. The diverse functions of histone acetyltransferase complexes. *Trends Genet.* 2003;19:321–329.
5. Verdin E, Dequiedt F, Kasler HG. Class II histone deacetylases: versatile regulators. *Trends Genet.* 2003;19:286–293.
6. Gusterson RJ, Jazrawi E, Adcock IM, Latchman DS. The transcriptional co-activators CREB-binding protein (CBP) and p300 play a critical role in cardiac hypertrophy that is dependent on their histone acetyltransferase activity. *J Biol Chem.* 2003;278:6838–6847.
7. Iezzi S, Di Padova M, Serra C, Caretti G, Simone C, Maklan E, Minetti G, Zhao P, Hoffman EP, Puri PL, Sartorelli V. Deacetylase inhibitors increase muscle cell size by promoting myoblast recruitment and fusion through induction of follistatin. *Dev Cell.* 2004;6:673–684.
8. Zhang CL, McKinsey TA, Chang S, Antos CL, Hill JA, Olson EN. Class II histone deacetylases act as signal-responsive repressors of cardiac hypertrophy. *Cell.* 2002;110:479–488.
9. Kook H, Lepore JJ, Gitler AD, Lu MM, Wing-Man Yung W, Mackay J, Zhou R, Ferrari V, Gruber P, Epstein JA. Cardiac hypertrophy and histone deacetylase-dependent transcriptional repression mediated by the atypical homeodomain protein Hop. *J Clin Invest.* 2003;112:863–871.
10. Antos CL, McKinsey TA, Dreitz M, Hollingsworth LM, Zhang CL, Schreiber K, Rindt H, Gorczynski RJ, Olson EN. Dose-dependent blockade to cardiomyocyte hypertrophy by histone deacetylase inhibitors. *J Biol Chem.* 2003;278:28930–28937.
11. Kuwahara K, Saito Y, Ogawa E, Takahashi N, Nakagawa Y, Naruse Y, Harada M, Hamanaka I, Izumi T, Miyamoto Y, Kishimoto I, Kawakami R, Nakanishi M, Mori N, Nakao K. The neuron-restrictive silencer element-neuron-restrictive silencer factor system regulates basal and endothelin 1-inducible atrial natriuretic peptide gene expression in ventricular myocytes. *Mol Cell Biol.* 2001;21:2085–2097.
12. Kaneda R, Toyota M, Yamashita Y, Koinuma K, Choi YL, Ota J, Kisanuki H, Ishikawa M, Takada S, Shimada K, Mano H. High-throughput screening of genome fragments bound to differentially acetylated histones. *Genes Cells.* 2004;9:1167–1174.
13. Yamamoto K, Dang QN, Kelly RA, Lee RT. Mechanical strain suppresses inducible nitric-oxide synthase in cardiac myocytes. *J Biol Chem.* 1998;273:11862–11866.
14. Kent WJ. BLAT–the BLAST-like alignment tool. *Genome Res.* 2002;12: 656–664.
15. Rat Genome Sequencing Project Consortium. Genome sequence of the Brown Norway rat yields insights into mammalian evolution. *Nature.* 2004;428:493–521.
16. Marks AR. Cardiac intracellular calcium release channels: role in heart failure. *Circ Res.* 2000;87:8–11.
17. Kapinya KJ, Harms U, Harms C, Blei K, Katchanov J, Dirnagl U, Hortnagl H. Role of NAD(P)H:quinone oxidoreductase in the progression of neuronal cell death in vitro and following cerebral ischaemia in vivo. *J Neurochem.* 2003;84:1028–1039.
18. Shawber C, Nofziger D, Hsieh JJ, Lindsell C, Bogler O, Hayward D, Weinmaster G. Notch signaling inhibits muscle cell differentiation through a CBF1-independent pathway. *Development.* 1996;122: 3765–3773.
19. Henderson C, Brancolini C. Apoptotic pathways activated by histone deacetylase inhibitors: implications for the drug-resistant phenotype. *Drug Resist Updat.* 2003;6:247–256.
20. Chen QM, Tu VC, Wu Y, Bahl JJ. Hydrogen peroxide dose dependent induction of cell death or hypertrophy in cardiomyocytes. *Arch Biochem Biophys.* 2000;373:242–248.
21. Onan D, Pipolo L, Yang E, Hannan RD, Thomas WG. Urotensin II promotes hypertrophy of cardiac myocytes via mitogen-activated protein kinases. *Mol Endocrinol.* 2004;18:2344–2354.
22. Fingert JH, Heon E, Liebmann JM, Yamamoto T, Craig JE, Rait J, Kawase K, Hoh ST, Buys YM, Dickinson J, Hockey RR, Williams-Lyn D, Trope G, Kitazawa Y, Ritch R, Mackey DA, Alward WL, Sheffield VC, Stone EM. Analysis of myocilin mutations in 1703 glaucoma patients from five different populations. *Hum Mol Genet.* 1999;8: 899–905.
23. Bernstein BE, Kamal M, Lindblad-Toh K, Bekiranov S, Bailey DK, Huebert DJ, McMahon S, Karlsson EK, Kulbokas EJ 3rd, Gingeras TR, Schreiber SL, Lander ES. Genomic maps and comparative analysis of histone modifications in human and mouse. *Cell.* 2005;120:169–181.
24. Weinmann AS, Yan PS, Oberley MJ, Huang TH, Farnham PJ. Isolating human transcription factor targets by coupling chromatin immunoprecipitation and CpG island microarray analysis. *Genes Dev.* 2002;16:235–244.
25. Turner BM, O'Neill LP. Histone acetylation in chromatin and chromosomes. *Semin Cell Biol.* 1995;6:229–236.
26. Strahl BD, Allis CD. The language of covalent histone modifications. *Nature.* 2000;403:41–45.

ELSEVIER

European Journal of Cancer 41 (2005) 2170–2175

European Journal of Cancer

www.ejconline.com

Retroviral expression screening of oncogenes in pancreatic ductal carcinoma

Hiroyuki Kisanuki [a], Young Lim Choi [a], Tomoaki Wada [a], Ryozo Moriuchi [b], Shin-ichiro Fujiwara [a], Ruri Kaneda [a], Koji Koinuma [a], Madoka Ishikawa [a], Shuji Takada [a], Yoshihiro Yamashita [a], Hiroyuki Mano [a,c,*]

[a] *Division of Functional Genomics, Jichi Medical School, 3311-1 Yakushiji, Kawachigun, Tochigi 329-0498, Japan*
[b] *Department of Molecular Microbiology and Immunology, Nagasaki University Graduate School of Medicine, Nagasaki, Japan*
[c] *CREST, Japan Science and Technology Agency, Saitama, Japan*

Received 4 March 2005; received in revised form 3 May 2005; accepted 10 May 2005
Available online 25 August 2005

Abstract

Pancreatic ductal carcinoma (PDC) remains one of the most intractable malignancies in humans. In order to clarify the molecular events underlying the carcinogenesis in PDC, we constructed a retroviral cDNA expression library from a PDC cell line, and used it to screen transforming genes in PDC by a focus formation assay with mouse 3T3 fibroblasts. We could obtain a total of 30 transformed cell foci in the screening, and one of the cDNA inserts harvested from such cell clones turned out to encode a wild-type human ARAF1. Unexpectedly, a long terminal repeat-driven overexpression of *ARAF1* mRNA was confirmed to induce transformed foci in fibroblasts. The oncogenic potential of ARAF1 was examined by injecting the transformed fibroblasts into athymic nude mice. Importantly, *ARAF1* mRNA was highly expressed in pancreatic ductal cell specimens purified from patients with PDC. These results have unveiled the transforming potential of ARAF1 protein, and also suggest that quantity of intracellular ARAF1 may be important in carcinogenesis of various human cancers.

Keywords: Pancreatic ductal cell carcinoma; Retrovirus; ARAF1; cDNA library; Oncogene

1. Introduction

Pancreatic ductal carcinoma (PDC) originates from pancreatic ductal cells, and is one of the most intractable malignancies in humans [1,2]. Effective therapy for PDC is hampered by the lack of specific clinical symptoms. At the time of diagnosis, most patients are no longer candidates for surgical resection, and, even in individuals who do undergo such surgery, the 5-year survival rate is only 20–30% [1].

Vast efforts have been made to elucidate molecular events responsible for the carcinogenesis of PDC. Mutations of *TP53* gene can be, for instance, found in PDC specimens [3], and in the intraductal *in situ* regions as well [4]. Similarly, inactivation has been found for other tumour-suppressor genes, such as DPC, RB1 and p16 [5].

As for oncogenes, activating mutations in the *KRAS2* gene has been reported to be frequently associated with PDC [6]. The same *KRAS2* mutations could be, however, found in the samples for chronic pancreatitis [7], making their pathogenetic role uncertain. Additionally, an increased telomerase activity was shown to be present only in PDC, but not in nonmalignant pancreatic disorders [8]. Again, however, others could detect an elevated telomerase activity in chronic pancreatitis and normal

* Corresponding author. Tel.: +81 285 58 7449; fax: +81 285 44 7322.
E-mail address: hmano@jichi.ac.jp (H. Mano).

0959-8049/$ - see front matter © 2005 Elsevier Ltd. All rights reserved.
doi:10.1016/j.ejca.2005.05.014

pancreas [9]. Therefore, it is yet to be revealed which transforming genes truly promote a clonal growth of pancreatic ductal cells.

For an efficient isolation of tumour-promoting genes in PDC, it would be desirable to conduct functional screening based on transforming ability. Focus formation assays with mouse 3T3 fibroblasts have been highly successful for the identification of oncogenes in human cancer [10]. In such screening, genomic DNA is isolated from cancer specimens, and used to transfect 3T3 cells to obtain transformed cell foci. It should be noted, however, that, since expression of any genes in these experiments are driven by their own promoters/enhancers, oncogenes in PDC can exert their effects in 3T3 cells only when the promoter/enhancer regions of such genes are active in fibroblasts, which is not always guaranteed.

To ensure the sufficient expression of cDNAs in 3T3 cells, their transcription should be regulated by an exogenous promoter fragment. We have therefore constructed a retroviral cDNA expression library from a PDC cell line, MiaPaCa-2, which was used to infect 3T3 cells. In the preparation of cDNA library, we further took advantage of the SMART polymerase chain reaction (PCR) system (Clontech, Palo Alto, CA), which preferentially amplifies full-length cDNAs. A focus formation assay with the library resulted in an identification of a transforming *ARAF1* gene.

2. Materials and methods

2.1. Cells and culture

MiaPaCa-2, Capan-2, PANC-1, 3T3, and BOSC23 [11] cell lines were obtained from American Type Culture Collection, and maintained in Dulbecco's modified Eagle medium/F12 (DMEM/F12; Invitrogen, Carlsbad, CA) containing 10% fetal bovine serum (Invitrogen) and 2 mM L-glutamine.

The fresh clinical specimens were obtained from patients who gave informed consent, and the study was approved by the institutional review board of Jichi Medical School. Cells were collected from the pancreatic juice by centrifugation, labeled with anti-MUC1 antibody [12] (Novocastra Laboratories, Newcastle upon Tyne, UK), and subjected to chromatography on a miniMACS magnetic cell separation column (Miltenyi Biotec, Auburn, CA) [13]. The purity of the resultant $MUC1^+$ cell fraction was confirmed by staining with Wright Giemmsa solutions and microscopy examination for each case (data not shown).

2.2. Retrovirus library construction

Total RNA was extracted from MiaPaCa-2 cells by an RNeasy Mini column with RNase-free DNase (Qiagen, Valencia, CA), and the first strand cDNA was synthesized by PowerScript reverse transcriptase (Clontech) with SMART IIA oligonucleotide and CDS primer IIA (both from Clontech). The cDNAs were then amplified for 12 cycles with 5′ PCR primer IIA according to the instruction of the SMART PCR cDNA synthesis kit (Clontech) except a substitution of LA Taq polymerase (Takara Bio, Shiga, Japan) for Advantage 2 DNA polymerase provided with the kit. Resultant cDNAs were treated with proteinase K, blunt-ended by T4 DNA polymerase, and ligated to the BstXI-adaptor (Invitrogen). Unbound adaptors were removed through the cDNA size fractionation column (Invitrogen), and the cDNAs were finally ligated to the pMXS retroviral plasmid (a kind gift of Dr. T. Kitamura at Institute of Medical Science, University of Tokyo) [14] digested with BstXI. The pMXS-cDNA plasmids were introduced into ElecroMax DH10B cells (Invitrogen) with electroporation.

2.3. Focus formation assay

Generation of recombinant retroviral library and focus formation assay was conducted as described previously [15]. Briefly, BOSC23 cells were transfected with Lipfectamin reagent (Invitrogen) and 2 μg of retroviral plasmid together with 0.5 μg of pGP plasmid 0.5 μg of pE-eco plasmid (both from Takara Bio). Two days after the transfection, polybrene (Sigma, St. Louis, MI) was added to the culture supernatant at a concentration of 4 μg/ml, and the supernatant was subsequently used to infect 3T3 cells for 48 h. For the focus formation assay, the culture medium of 3T3 cells was then changed to DMEM-high glucose (Invitrogen) supplemented with 5% calf serum and 2 mM L-glutamine. Transformed foci were picked up after 3 weeks of culture. Genomic DNA was extracted from each transformed focus, and was subjected to PCR with 5′ PCR primer IIA (Clontech) and LA Taq polymerase for 50 cycles of 98 °C for 20 s and 68 °C for 6 min. Amplified genome fragments were purified for nucleotide sequencing. For tumorgenicity assay in nude mice, transformed 3T3 cells were injected into each shoulder of nu/nu Balb-c mice (6 weeks old). Tumour formation was assessed after 4 weeks.

2.4. "Real-time" RT-PCR

Portions of oligo(dT)-primed cDNA were subjected to PCR with a QuantiTect SYBR Green PCR Kit (Qiagen). The amplification protocol was comprised of incubations at 94 °C for 15 s, 57 °C for 30 s, and 72 °C for 60 s. Incorporation of the SYBR Green dye into PCR products was monitored in real time with an ABI PRISM 7900HT sequence detection system (PE Applied Biosystems, Foster City, CA), thereby allowing determination of the threshold cycle (C_T) at which exponential amplification of products

begins. The C_T values for cDNAs corresponding to the β-actin gene (*ACTB*) and to the *ARAF1* gene were used to calculate the abundance of the latter mRNA relative to that of the former. The oligonucleotide primers for PCR were as follows: 5′-CCATCATGAAGTGTGACGTGG-3′ and 5′-GTCCGCCTAGAAGCATTTGCG-3′ for *ACTB*, and 5′-ACTACCTCCATGCCAAGAACATCA-3′ and 5′-GACGTCTGACTGGAAGCTGTAGGG-3′ for *ARAF1*.

3. Results

3.1. Screening with focus formation assay

From mRNA of MiaPaCa-2 cells, full-length cDNAs were selectively amplified and ligated to a retroviral vector pMXS. We could obtain a total of 2.1×10^6 colony forming units (cfu) of independent plasmid clones. Thirty clones were randomly selected from the library, and examined for the incorporated cDNAs. Twenty-seven (90%) out of the 30 clones contained inserts with an average length of 2.05 kbp.

By introducing the plasmid DNA into a packaging cell line, we generated a recombinant ecotropic retrovirus library that was subsequently used to infect mouse 3T3 fibroblasts. Infection experiments were repeated for a total of 6 times. After 3 weeks of culture, 30 transformed foci were observed (Fig. 1(b)). No foci could be found among the cells infected with an empty virus (Fig. 1(a)), while numerous foci were easily identified in the cells infected with a virus expressing v-Ras oncoprotein (Fig. 1(c)).

Each focus was isolated, expanded independently, and was subject to the extraction of genomic DNA. We then tried to recover retroviral inserts from the genomic DNA by PCR amplification with the primer used originally to amplify the cDNAs in the construction of the library. In most cases, two to three DNA fragments were recovered from each genome (Fig. 2(a)), implying a multiple retroviral infection on the recipient 3T3 cells.

We obtained a total of 56 cDNA fragments by PCR, all of which were subjected to nucleotide sequencing from both ends. Screening of the cDNA sequences against human genome sequence database assembled as of July 2003 by the Genome Bioinformatics Group of the University of California at Santa Cruz (http://genome.ucsc.edu) revealed that the 56 fragments correspond to 13 independent genes, eleven of which could be matched at >95% identity to the human genome sequence (Table 1). Among the 11 genes, 7 of them were known genes while the rest 4 were unknown. Each cDNA clone was ligated to pMXS in both directions, and a recombinant retrovirus was generated from each resultant plasmid. Transforming ability of the cDNAs was thus confirmed by a focus formation assay with the recombinant virus.

Focus formation assays were conducted for the 26 independent viruses (all 13 independent genes for both directions), and one of them, expressing ARAF1 protein (GenBank accession number, NM_001654), gave transformed foci in repeated experiments. ARAF1 belongs to

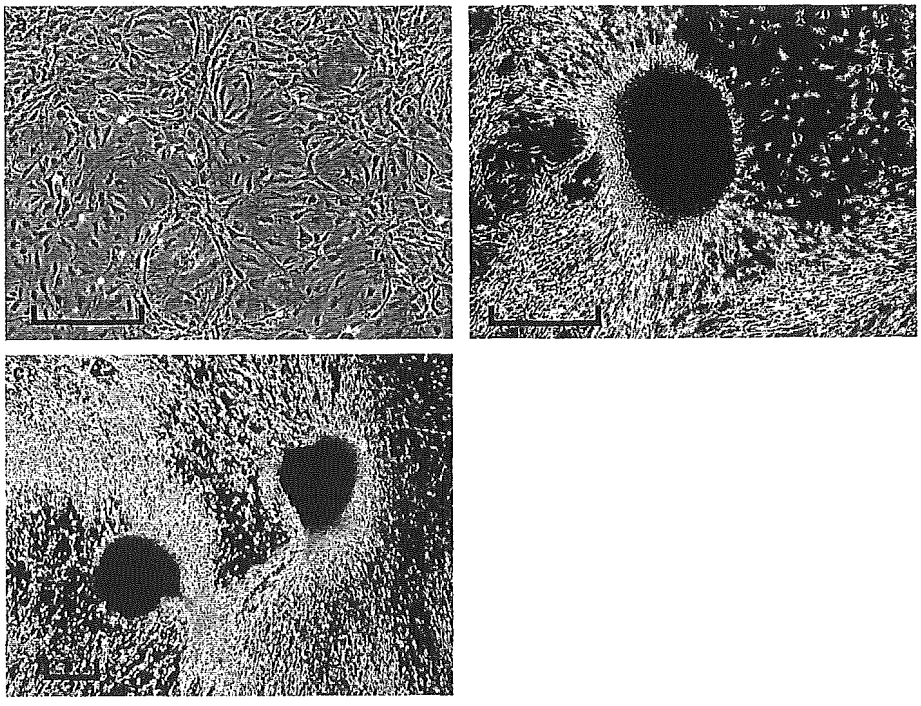

Fig. 1. Focus formation assay with retroviral library. Mouse 3T3 cells were infected with (a) an empty virus, (b) retroviruses from the MiaPaCa-2 library, or (c) a retrovirus expressing v-Ras as a positive control. Pictures were taken after 3 weeks of culture. Scale bar, 100 μm.

Table 1
cDNAs isolated from 3T3 transformants

Clone #	Gene symbol	GenBank number	Covering full ORF
1	Unknown	AK026325	ND
2	No homologues sequences	ND	ND
3	Unknown	AF318370	Yes
4	PITPNM1	NM_004910	No
5	Unknown	BC022099	Yes
6	DECR2	NM_020664	Yes
7	ARAF1	NM_001654	Yes
8	BCLG	NM_138724	No
9	No homologues sequences	ND	ND
10	Unknown	AL607122	ND
11	JAG1	NM_000214	Yes
12	MRPL43	NM_176792	Yes
13	PLOD3	NM_001084	No

ORF, open reading frame; ND, not determined.

the RAF family of serine/threonine kinases, and phosphorylates MEK1 [16]. It had not been known whether an overexpression of wild ARAF1 protein has a transforming activity.

3.2. *ARAF1* as an oncogene

We thus determined the whole nucleotide sequence of our *ARAF1* cDNA (cDNA clone ID #7). The sequence is 2441 bp, and contains an open reading frame (spanning nucleotide position 126–1943) encoding a protein of 606 amino acids, which is identical to ARAF1 (Fig. 2(b)). Within the protein-coding region, there is only one nucleotide mutation compared to the published *ARAF1* cDNA sequence; a "T" at nucleotide position 1550 in the reported sequence (NM_001654) is replaced with a "C" in our sequence. The codon sequence "TTG" at the amino acid position 450 of ARAF1 is thus changed to "CTG" in our cDNA. However, both codons encode the same leucine residue, and thus the mutation does not affect the protein sequence.

To confirm that mere overexpression of wild ARAF1 protein has a transforming activity, we repeated the focus formation assay with the retrovirus generated from our *ARAF1* cDNA. As shown in Fig. 2(c), the recombinant virus reproducibly induced transformed foci (30–50 foci per microgram of the input plasmid) in the recipient 3T3 cells. The transforming ability of ARAF1 was also tested by the tumorgenicity assay with athymic nude mice. The 3T3 cells infected with the empty virus or retrovirus expressing ARAF1 or v-Ras were inoculated subcutaneously into nude mice. As shown in Fig. 2(d), tumour formation was observed in all mice for the latter 2 cases, arguing that ARAF1 has oncogenic potential.

3.3. Expression of *ARAF1* in PDC

We finally measured the expression level of *ARAF1* mRNA in PDC by the quantitative real-time reverse

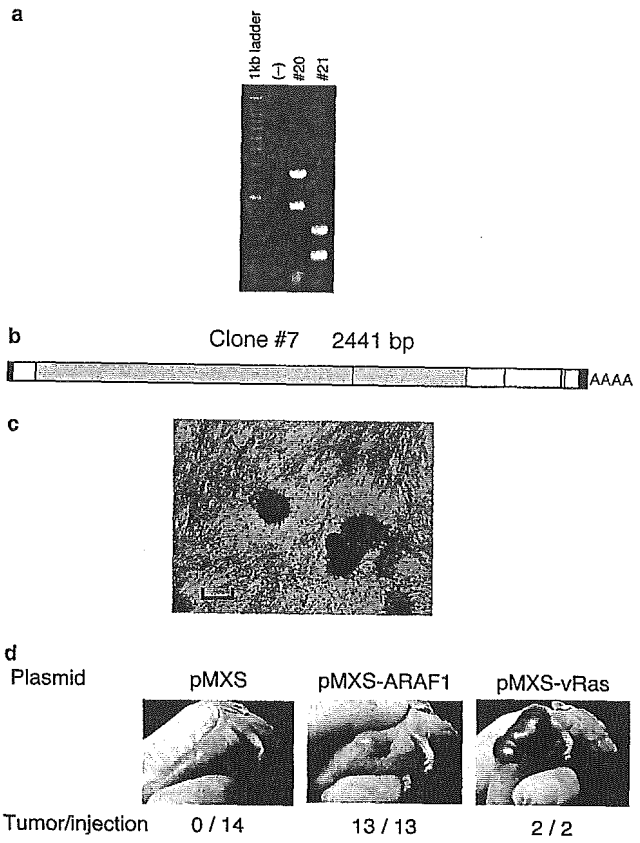

Fig. 2. Identification of the transforming *ARAF1* gene. (a) Genomic DNAs isolated from the transformed foci (cell clone ID #20 and #21) were subjected to PCR. A PCR without DNA template was also conducted as a negative control (−). DNA size markers (1 kb DNA ladder; Invitrogen) are electrophoresed at the left. (b) A 3T3 clone yielded a PCR product of 2441 bp long (cDNA clone ID #7). The cDNA has a protein-coding region (gray) for 606 amino acids that was identical to human ARAF1 protein. Nucleotides that did not match the published *ARAF1* cDNA are indicated by red lines. (c) Our ARAF1 cDNA was ligated to pMXS, and used to generate recombinant virus. Infection with the virus induced multiple transformed foci in 3T3 cells. Scale bar, 100 μm. (d) 3T3 cells (5×10^5) were cultured for two days with retrovirus made from pMXS, pMXS-ARAF1 or pMXS-vRas plasmid, and were injected subcutaneously into nu/nu mice. Tumour formation was examined after 4 weeks.

transcription (RT)-PCR method. As shown in Fig. 3, all 3 PDC cell lines express similar amounts of *ARAF1* mRNA. In addition, we quantified *ARAF1* mRNA in human clinical specimens. Pancreatic juice from patients with PDC contains cancer cells (transformed ductal cells) in addition to normal ductal cells and blood cells. The former two fractions were purified, by an affinity column for MUC1 surface protein [12], from pancreatic juice of PDC patients ($n = 14$). Such purified fractions should be highly enriched for PDC cells [13]. Similar MUC1-positive fractions were also purified from the pancreatic juice of healthy individuals ($n = 7$). Quantification of *ARAF1* mRNA revealed that its mRNA level was highly elevated in six out of the 14 patient, but not in the specimens from healthy individuals. These data

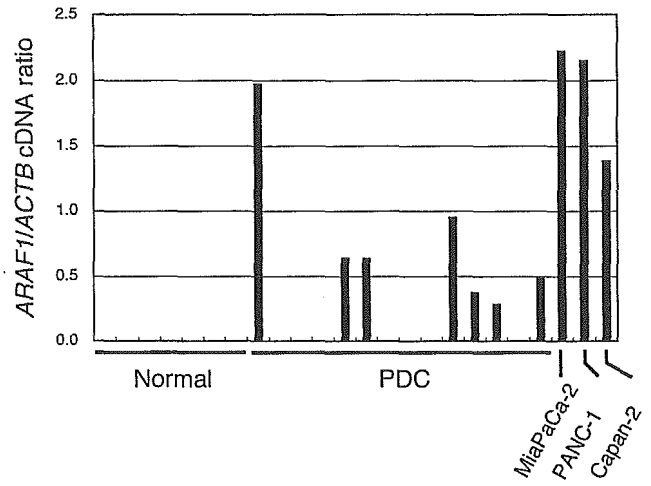

Fig. 3. Quantification of *ARAF1* mRNA. Complementary DNA was prepared from PDC cell lines (MiaPaCa-2, PANC-1 and Capan-2) or $MUC1^+$ ductal cell preparations purified from healthy individuals (Normal) or patients with PDC, and were then subjected to real-time RT-PCR analysis with primers specific for the *ARAF1* or *ACTB* genes. The ratio of the abundance of *ARAF1* mRNA to that of *ACTB* mRNA was calculated as 2^n, where n is the C_T value for *ACTB* cDNA minus the C_T value for *ARAF1* cDNA.

indicate that the transcription of *ARAF1* is selectively activated in PDC cells.

4. Discussion

In this manuscript, we have constructed a retroviral cDNA expression library of PDC. Since 90% (27/30) of the viral plasmids carried cDNA inserts and since the overall clone number was >2 millions, our library should cover nearly all transcriptome in MiaPaCa-2 cells.

RAF family is composed of RAF1, ARAF1 and BRAF in humans. All these serine/threonine kinases are believed to act downstream of RAS-family proteins, and to phosphorylate and regulate downstream MAP kinase kinases (MAPKKs). Many studies have revealed transforming potentials of RAF family proteins. RAF was originally identified as a cellular homologue of viral oncoprotein, v-Raf [17]. Deletion of amino-terminal regions unmasks the transforming ability of RAF1 [18] and ARAF1 [19]. On the other hand, somatic point mutations have been found in the *BRAF* gene among clinical specimens of colorectal carcinoma [20]. Such mutations were shown to induce transforming activity in BRAF protein. In contrast to *BRAF*, somatic point mutations are rarely found in *ARAF1* gene [21].

Overexpression of wild forms of RAF1 or BRAF failed to exert a transforming activity [18,20]. Although deletion/truncation of amino terminal regions of ARAF1 induced transformed foci in 3T3 fibroblasts [22] and abrogated cytokine-dependency in hematopoietic cells [19], it has not been tested whether wild ARAF1 protein has transforming potential. In this manuscript, however, it was unexpectedly revealed that a long terminal repeat-driven expression of ARAF1 induces transformed foci in 3T3 cells, which subsequently generated tumours in immunocompromised mice. Therefore, it has been unveiled here that an overexpression of wild ARAF1 is directly linked with cellular transformation process.

These data also indicate the importance of measuring protein/mRNA amounts of ARAF1 in various human cancers. In this context, it was interesting to find a high expression of *ARAF1* mRNA in fresh clinical specimens of PDC. Our findings shed new light on the understanding of RAF family kinases, and open up the possibility that ARAF is involved in carcinogenesis in human cancers through a previously unexpected mechanism.

Conflict of interest statement

None declared.

Acknowledgments

This work was supported in part by a grant for Third-Term Comprehensive Control Research for Cancer from the Ministry of Health, Labor, and Welfare of Japan; and a grant for "High-Tech Research Center" Project for Private Universities: Matching Fund Subsidy (2002–2006) from the Ministry of Education, Culture, Sports, Science, and Technology of Japan.

References

1. Bornman PC, Beckingham IJ. Pancreatic tumours. *Br Med J* 2001, **322**, 721–723.
2. Rosewicz S, Wiedenmann B. Pancreatic carcinoma. *Lancet* 1997, **349**, 485–489.
3. Goggins M, Kern SE, Offerhaus JA, *et al.* Progress in cancer genetics: lessons from pancreatic cancer. *Ann Oncol* 1999, **10**(Suppl. 4), 4–8.
4. Barton CM, Staddon SL, Hughes CM, *et al.* Abnormalities of the p53 tumour suppressor gene in human pancreatic cancer. *Br J Cancer* 1991, **64**, 1076–1082.
5. Bramhall SR. The use of molecular technology in the differentiation of pancreatic cancer and chronic pancreatitis. *Int J Pancreatol* 1998, **23**, 83–100.
6. Tada M, Omata M, Ohto M. Clinical application of ras gene mutation for diagnosis of pancreatic adenocarcinoma. *Gastroenterology* 1991, **100**, 233–238.
7. Yanagisawa A, Ohtake K, Ohashi K, *et al.* Frequent c-Ki-ras oncogene activation in mucous cell hyperplasias of pancreas suffering from chronic inflammation. *Cancer Res* 1993, **53**, 953–956.
8. Hiyama E, Kodama T, Shinbara K, *et al.* Telomerase activity is detected in pancreatic cancer but not in benign tumours. *Cancer Res* 1997, **57**, 326–331.
9. Uehara H, Nakaizumi A, Tatsuta M, *et al.* Diagnosis of pancreatic cancer by detecting telomerase activity in pancreatic

juice: comparison with K-ras mutations. *Am J Gastroenterol* 1999, **94**, 2513–2518.
10. Aaronson SA. Growth factors and cancer. *Science* 1991, **254**, 1146–1153.
11. Pear WS, Nolan GP, Scott ML, *et al.* Production of high-titer helper-free retroviruses by transient transfection. *Proc Natl Acad Sci USA* 1993, **90**, 8392–8396.
12. Terada T, Ohta T, Sasaki M, *et al.* Expression of MUC apomucins in normal pancreas and pancreatic tumours. *J Pathol* 1996, **180**, 160–165.
13. Yoshida K, Ueno S, Iwao T, *et al.* Screening of genes specifically activated in the pancreatic juice ductal cells from the patients with pancreatic ductal carcinoma. *Cancer Sci* 2003, **94**, 263–270.
14. Onishi M, Kinoshita S, Morikawa Y, *et al.* Applications of retrovirus-mediated expression cloning. *Exp Hematol* 1996, **24**, 324–329.
15. Yoshizuka N, Moriuchi R, Mori T, *et al.* An alternative transcript derived from the trio locus encodes a guanosine nucleotide exchange factor with mouse cell-transforming potential. *J Biol Chem* 2004, **279**, 43998–44004.
16. Wu X, Noh SJ, Zhou G, *et al.* Selective activation of MEK1 but not MEK2 by A-Raf from epidermal growth factor-stimulated Hela cells. *J Biol Chem* 1996, **271**, 3265–3271.
17. Bonner TI, Kerby SB, Sutrave P, *et al.* Structure and biological activity of human homologs of the raf/mil oncogene. *Mol Cell Biol* 1985, **5**, 1400–1407.
18. Ishikawa F, Sakai R, Ochiai M, *et al.* Identification of a transforming activity suppressing sequence in the c-raf oncogene. *Oncogene* 1988, **3**, 653–658.
19. Hoyle PE, Moye PW, Steelman LS, *et al.* Differential abilities of the Raf family of protein kinases to abrogate cytokine dependency and prevent apoptosis in murine hematopoietic cells by a MEK1-dependent mechanism. *Leukemia* 2000, **14**, 642–656.
20. Davies H, Bignell GR, Cox C, *et al.* Mutations of the BRAF gene in human cancer. *Nature* 2002, **417**, 949–954.
21. Lee JW, Soung YH, Kim SY, *et al.* Mutational analysis of the ARAF gene in human cancers. *APMIS* 2005, **113**, 54–57.
22. Beck TW, Huleihel M, Gunnell M, *et al.* The complete coding sequence of the human A-raf-1 oncogene and transforming activity of a human A-raf carrying retrovirus. *Nucleic Acids Res* 1987, **15**, 595–609.

Carcinogenesis vol.26 no.12 pp.2078–2085, 2005
doi:10.1093/carcin/bgi184
Advance Access publication July 20, 2005

Screening for genomic fragments that are methylated specifically in colorectal carcinoma with a methylated *MLH1* promoter

Koji Koinuma[1,2], Ruri Kaneda[1], Minoru Toyota[3], Yoshihiro Yamashita[1], Shuji Takada[1], Young Lim Choi[1], Tomoaki Wada[1], Masaki Okada[2], Fumio Konishi[4], Hideo Nagai[2] and Hiroyuki Mano[1,5,*]

[1]Division of Functional Genomics and [2]Department of Surgery, Jichi Medical School, Tochigi 329-0498, Japan, [3]Department of Molecular Biology, Cancer Research Institute, Sapporo Medical University, Hokkaido 060-8556, Japan, [4]Department of Surgery, Omiya Medical Center of Jichi Medical School, Saitama 330-8503, Japan and [5]CREST, Japan Science and Technology Agency, Saitama 332-0012, Japan

*To whom correspondence should be addressed. Tel: +81 285 58 7449; Fax: +81 285 44 7322;
E-mail: hmano@jichi.ac.jp

A subset of colorectal carcinomas (CRCs) is associated with microsatellite instability (MSI) of the genome. Although extensive methylation of CpG islands within the promoter regions of DNA mismatch repair genes such as *MLH1* is thought to play a central role in tumorigenesis for MSI-positive sporadic CRCs, it has been obscure whether such aberrant epigenetic regulation occurs more widely and affects other cancer-related genes *in vivo*. Here, by using methylated CpG island amplification coupled with representational difference analysis (MCA–RDA), we screened genomic fragments that are selectively methylated in CRCs positive for *MLH1* methylation, resulting in the identification of hundreds of CpG islands containing genomic fragments. Methylation status of such CpG islands was verified for 28 genomic clones in 8 CRC specimens positive for *MLH1* methylation and the corresponding paired normal colon tissue as well as in 8 CRC specimens negative for methylation. Many of the CpG islands were preferentially methylated in the *MLH1* methylation-positive CRC specimens, although methylation of some of them was more widespread. These data provide insights into the complex regulation of the methylation status of CpG islands in CRCs positive for MSI and *MLH1* methylation.

Introduction

Colorectal carcinoma (CRC) is one of the leading causes of cancer death in humans. Evidence indicates the existence of two major types of genomic instability in CRCs: chromosomal instability and microsatellite instability (MSI) (1). Whereas chromosomal instability is associated with an abnormal DNA content (such as aneuploidy), inactivation of the tumor suppressor gene *TP53*, and activation of oncogenes (2), MSI is associated with defects in the DNA mismatch repair (MMR) system that result in frameshift mutations in microsatellite repeats, and thereby affect the structure of genes containing such repeats (3).

Although germ-line mutations of MMR genes have been detected in the genome of individuals with hereditary non-polyposis colorectal cancer (4–6), many sporadic CRCs positive for MSI are associated with epigenetic silencing of non-mutated MMR genes (7,8). MSI-positive CRCs are characterized by specific clinicopathologic features and gene mutations. Such tumors occur with a higher frequency in women than in men, develop in the right side of the colon, and manifest a mucinous or poorly differentiated histopathology. Many of the CpG dinucleotides within the promoter region of the MMR gene *MLH1* are methylated in MSI-positive CRCs (9,10), and the *BRAF* gene frequently contains activating mutations in these cancers (11–13). Some genomic fragments have been found to be methylated specifically in such CRCs (7), and an entity of CRC with a CpG island methylator phenotype (CIMP) has been proposed (14). However, the profiles of genes and genomic fragments that become methylated in CRC specimens positive for *MLH1* methylation have remained uncharacterized.

With the use of methylated CpG island amplification coupled with representational difference analysis (MCA–RDA) (15), we have now performed a global screening of pooled genomic DNA from CRC specimens positive or negative for *MLH1* methylation in order to identify differentially methylated genomic fragments. With this approach, we identified hundreds of CpG islands whose methylation was specific to CRCs with a methylated *MLH1* promoter.

Abbreviations: CRC, colorectal carcinoma; COBRA, combined bisulfite restriction analysis; CIMP, CpG island methylator phenotype; EGF, epidermal growth factor; GDF, growth-differentiation factor; MSI, microsatellite instability; MMR, mismatch repair; PCR, polymerase chain reaction; TGF-β, transforming growth factor-β.

Materials and methods

Tumor specimens and cell lines

Tumor specimens were obtained from patients with sporadic CRC who underwent surgical treatment in Jichi Medical School Hospital. Informed consent was obtained from each patient, and the study was approved by the ethics committee of Jichi Medical School. Normal portion of colon tissue was excised from a region >5 cm distant from the cancerous region in every case. Genomic DNA was extracted with the use of a QIAmp DNA Mini kit (Qiagen, Valencia, CA). The MSI status of each tumor was determined on the basis of analysis of nine microsatellite repeat loci as previously described (8). The methylation status of the *MLH1* promoter was also examined in each sample (11).

Colon carcinoma cell lines (Caco-2, HCT116, SW480) were obtained from American Type Culture Collection (Manassas, VA). Caco2 cells were cultured in Dulbecco's modified Eagle's medium (DMEM)-F12 (Invitrogen, Carlsbad, CA) supplemented with 10% fetal bovine serum (FBS) (Invitrogen) and 2 mM L-glutamine. HCT116 and SW480 cells were maintained in McCoy's 5A medium (Invitrogen) and Leibovitz's L-15 medium (Invitrogen), both supplemented with 10% FBS, respectively.

MCA–RDA

Genomic DNA from four tumor specimens positive for *MLH1* methylation was mixed and used as a 'tester' sample, whereas that from four specimens negative for *MLH1* methylation was used as a 'driver.' MCA–RDA was performed with the two pooled DNA samples as previously described (15). In brief, both the tester and the driver DNA samples (5 μg of each) were digested first with the SmaI endonuclease (New England Biolabs, Beverly, MA) and then with

XmaI (New England Biolabs), and the resulting fragments were ligated to the RMCA adapter (15). Amplification of methylated CpG islands was achieved by polymerase chain reaction (PCR) with the RMCA24 primer. The amplified fragments of the tester-DNA and driver-DNA were digested with XmaI and SmaI, respectively. The tester amplicons were then ligated to the JMCA adapter and subjected to annealing with an excess amount of the driver amplicons. PCR with the JMCA24 primer then amplified only the tester-specific amplicons. Another round of amplification was performed with the NMCA adapter and the NMCA24 primer (15). The final products were digested with XmaI and ligated into XmaI-digested pBlueScript (Stratagene, La Jolla, CA) for nucleotide sequencing.

Combined bisulfite restriction analysis (COBRA)

The methylation status of isolated clones was tested by the COBRA method (16). The genomic DNA was denatured, incubated for 16 h at 55°C in 3.1 M sodium bisulfite, and then subjected to PCR to amplify CpG islands. The PCR products were digested with a restriction endonuclease, and the resulting fragments were fractionated by polyacrylamide gel electrophoresis (PAGE). The gel was stained with SYBR Green I (Takara Bio, Shiga, Japan) and scanned with an LAS3000 imaging system (Fuji Film, Tokyo, Japan). Genomic fragments were determined to be positive for CpG methylation if $\geq$10% of the PCR products were cleaved by the restriction endonuclease. The PCR primers and endonucleases used for COBRA are shown in the Supplementary Table online.

For bisulfite sequencing of the *BMP3* promoter, genomic DNA isolated from cancer specimens or cell lines was treated with sodium bisulfite (11) and then subjected to PCR with the primers 5′-AGTTAGAGAGYGAAAGAATTAAG-3′ and 5′-ATACAACRAAATAACRACCAACC-3′. The PCR product was ligated into pGEMT-easy (Promega, Madison, WI).

Real-time reverse transcription-polymerase chain reaction (RT–PCR)

Total RNA was prepared from tester or driver samples with an RNeasy Mini column (Qiagen), treated with RNase-free DNase (Qiagen), and subjected to reverse transcription with PowerScript reverse transcriptase (BD Biosciences Clontech, San Jose, CA) and an oligo(dT) primer. Portions of the resulting cDNAs were subjected to PCR with a QuantiTect SYBR Green PCR kit (Qiagen). The amplification protocol comprised incubations at 94°C for 15 s, 63°C (64°C for *KIT* cDNA) for 30 s, and 72°C for 60 s. Incorporation of the SYBR Green dye into PCR products was monitored in real time with an ABI PRISM 7900HT sequence detection system (PE Applied Biosystems, Foster City, CA), thereby allowing determination of the threshold cycle (C_T) at which exponential amplification of PCR products begins. The C_T values for DNA molecules corresponding to the β-actin gene (*ACTB*) and to genomic fragments of interest were used to calculate the abundance of the latter relative to that of the former. The oligonucleotide primers for PCR were 5′-CCATCATGAAGTGTGACGTGG-3′ and 5′-GTCCGCCTAGAAGCATTTGCG-3′ for *ACTB*, 5′-AAGTCAACTCCTTGGCCATCTGT-3′ and 5′-TGGAAAAGGTAACCTCCTCTTTGG-3′ for the bone morphogenetic protein 3 gene (*BMP3*), and 5′-TGACGTCTGGTCCTATGGGATTT-3′ and 5′-TACATTTCAGCAGGTGCGTGTTC-3′ for *KIT*.

Results

MCA–RDA screening

A total of 249 cases with CRC were examined for their MSI status as well as for methylation in the promoter region of *MLH1*. The majority ($n = 213$) of the tumor specimens from these patients were negative for MSI, while the rest ($n = 36$) were MSI-positive. Also, most of them ($n = 226$) were shown to have no methylation within the *MLH1* promoter (unmethylated group), whereas the remainder ($n = 23$) had a methylated promoter (methylated group) (11). Altogether 16 patients were positive for MSI, but did not have a methylated *MLH1* promoter. On the other hand, three patients were negative for MSI despite the presence of the methylated *MLH1* promoter. The characteristics of the patients examined in the present study are summarized in Table I.

To isolate genes that were specifically methylated in the methylated group, we selected specimens from four men of each group: ID nos 2, 17, 20 and 77 (mean age, 70.0 years) from the methylated group, and ID nos 1, 8, 13 and 31 (mean age, 73.0 years) from the unmethylated group. We have excluded female subjects from the initial screening, since an intense methylation of one X chromosome in female cells may have yielded a large number of pseudopositive clones, methylation status of which may not have linked to the clinical classes, but to lyonization.

Table I. Patient characteristics

ID no.	*MLH1* methylation	MSI status	Age (years)	Sex	Dukes grade
2[a]	Yes	MSS	70	Male	A
17[a]	Yes	MSI	65	Male	B
20[a]	Yes	MSI	76	Male	B
77[a]	Yes	MSI	69	Male	A
225	Yes	MSI	83	Female	C
263	Yes	MSI	86	Female	C
280	Yes	MSI	83	Female	C
305	Yes	MSI	74	Male	B
318	Yes	MSI	76	Female	B
336	Yes	MSI	68	Male	B
413	Yes	MSI	69	Female	A
416	Yes	MSI	76	Female	B
1[a]	No	MSS	65	Male	A
8[a]	No	MSS	89	Male	B
13[a]	No	MSS	74	Male	B
31[a]	No	MSS	64	Male	B
238	No	MSS	74	Male	A
249	No	MSS	62	Male	B
255	No	MSS	69	Female	C
278	No	MSS	73	Male	C
295	No	MSS	71	Female	C
298	No	MSS	70	Male	D
307	No	MSS	80	Female	C
308	No	MSS	62	Male	B
481	No	MSS	59	Male	C

[a]Specimens used for MCA–RDA screening. MSS, microsatellite stable.

Equal amounts of genomic DNA isolated from the four selected tumor specimens of each group were mixed and subjected to MCA–RDA analysis, with the pooled DNA of the methylated group as the tester and that of the unmethylated group as the driver. A total of 384 clones were randomly picked up from the resultant MCA–RDA products, and digestion of the purified plasmid DNA with restriction endonucleases revealed that 294 out of the 384 clones carried the insert fragments. Nucleotide sequencing of such 294 clones indicated that 209 of the clones were found to contain CpG islands. Screening of human genome databases (http://www.ncbi.nlm.nih.gov/BLAST/ and http://genome.ucsc.edu/cgi-bin/hgBlat) with these sequences revealed that 186 of them were localized within or in close proximity to characterized or uncharacterized human genes (112 independent genes).

Candidate genes for differential methylation

The GenBank accession numbers and annotation information for the 112 genes identified by MCA–RDA are shown in Table II. Multiple clones were isolated for a single gene in 33 instances, whereas only one MCA–RDA product was obtained for the remaining genes. The genes listed in Table II were thus candidates for genes whose CpG islands are methylated in a manner dependent on *MLH1* methylation.

We then examined the methylation status of the isolated fragments mapped to the promoter regions. First, we tried to amplify individually by PCR all 70 fragments mapped to the promoter regions in Table II, and could successfully amplify 35 fragments from the pooled DNAs used in MCR–RDA.

Table II. Genes identified by MCA–RDA with CRCs positive or negative for *MLH1* methylation

Gene	GenBank accession no.	No. of MCA–RDA clones	Position of MCA–RDA clones	COBRA data
Homo sapiens, solute carrier family 38, member 3	BC042875	11	Promoter	N.D.
Homo sapiens hypothetical protein MGC29643[a]	AK075487	10	Promoter	compatible
Human progesterone receptor	M15716	6	Exon 1	N.D.
Homo sapiens alpha-1 type XV collagen	L25286	6	Promoter	N.D.
Homo sapiens K-Cl co-transporter KCC4	AF105365	5	Promoter	N.D.
Homo sapiens CGI-150 protein	AF151908	5	3′ region	N.D.
Homo sapiens cDNA FLJ37615	AK094934	4	3′ region	N.D.
Human mRNA and promoter DNA for progesterone receptor	X51730	3	Promoter	N.D.
Human arachidonate 12-lipoxygenase mRNA	M62982	3	Promoter	not compatible
Homo sapiens clone IMAGE:5173621	BC031660	3	Promoter	N.D.
Homo sapiens Ras and Rab interactor 1	BC014417	3	3′ region	N.D.
Homo sapiens papilin (PAPLN)[a]	BC042057	3	Promoter	compatible
Homo sapiens F-box and leucine-rich repeat protein 7 (FBXL7)[a]	AB020647	3	Promoter	compatible
Homo sapiens fibronectin type 3 and ankyrin repeat domains 1	BC024189	3	Promoter	not compatible
BX444427 *Homo sapiens* ADULT BRAIN *Homo sapiens* cDNA clone	BX444427	3	Promoter	N.D.
UI-H-BW0-aju-d-09-0-UI.s1 NCI_CGAP_Sub6 *Homo sapiens* cDNA clone	AW297872	2	N.D.	N.D.
Human dystrobrevin-delta	U26742	2	Near 5′ end	N.D.
Homo sapiens, clone IMAGE:5728979	BC035731	2	Promoter	compatible
Homo sapiens ras interactor (RIN1)	L36463	2	Promoter	N.D.
Homo sapiens partial mRNA for doublesex-mab-3 (DM) domain	AJ301580	2	Promoter	not compatible
Homo sapiens mRNA; cDNA DKFZp586D0619	AL834130	2	Promoter	N.D.
Homo sapiens mRNA for NTAK[a]	AB005060	2	Promoter	compatible
Homo sapiens mRNA for FLJ00396 protein	AK090474	2	3′ region	N.D.
Homo sapiens mRNA for dihydropyrimidinase related protein-3 (DPYSL3)[a]	D78014	2	Promoter	compatible
Homo sapiens hypothetical protein MGC35308	BC034775	2	Exon 1	N.D.
Homo sapiens hypothetical protein MGC33600	BC035022	2	N.D.	N.D.
Homo sapiens growth differentiation factor 7 (GDF7)[a]	AF522369	2	Promoter	compatible
Homo sapiens gene NXN encoding nucleoredoxin	NM_022463	2	N.D.	N.D.
Homo sapiens clone 24649	AF070591	2	3′ region	N.D.
Homo sapiens cDNA: FLJ21511	AK025164	2	Promoter	not compatible
Homo sapiens solute carrier family 30, member 10 (SLC30A10)[a]	AK090806	2	Promoter	compatible
Homo sapiens beta-parvin	AF237769	2	Promoter	N.D.
603031612F1 NIH_MGC_115 *Homo sapiens* cDNA clone IMAGE:5172891	BI489865	2	Promoter	N.D.
Mus musculus adult male spinal cord cDNA, clone:A330088B02	AK079637	1	N.D.	N.D.
Mus musculus 9.5 days embryo parthenogenote cDNA, clone:B130054P17	AK045275	1	N.D.	N.D.
Mus musculus 12 days embryo spinal ganglion cDNA, clone:D130032D18	AK051302	1	N.D.	N.D.
IL5-EN0086-281100-292-f08 EN0086 *Homo sapiens* cDNA	BF851362	1	N.D.	N.D.
Human receptor tyrosine kinase ligand LERK-7 precursor	U26403	1	Promoter	not compatible
Human solute carrier family 30, member 3 (SLC30A3)[a]	U76010	1	Promoter	compatible
Human platelet-derived growth factor receptor alpha	M21574	1	3′ region	N.D.
Human pephBGT-1 betaine-GABA transporter	U27699	1	3′ region	N.D.
Human oxytocin mRNA	M25650	1	Promoter	N.D.
Human mRNA for KIAA0222 gene	D86975	1	3′ region	N.D.
Human c-kit proto-oncogene (KIT)[a]	X06182	1	Promoter	compatible
Human cell 12-lipoxygenase	M35418	1	Promoter	N.D.
Human bone morphogenetic protein-3 (BMP3)[a]	M22491	1	Promoter	compatible
Human (clone hST3O-1) sialyltransferase	L29555	1	Promoter	N.D.
Homo sapiens, Similar to parathyroid hormone receptor 1	BC031578	1	3′ region	N.D.
Homo sapiens, potassium channel, subfamily K, member 13 (KCNK13)[a]	BC012779	1	Promoter	compatible
Homo sapiens, clone MGC:50339	BC043386	1	N.D.	N.D.
Homo sapiens, clone IMAGE:6041910	BC040712	1	Promoter	N.D.
Homo sapiens, clone IMAGE:5590527	BC040874	1	Promoter	N.D.
Homo sapiens Wilms tumor 1	BC032861	1	Promoter	not compatible
Homo sapiens TRALPUSH[a]	AF399708	1	Promoter	compatible
Homo sapiens Sry-related HMG-box protein	AF270652	1	Exon 1	N.D.
Homo sapiens sialyltransferase 4A, transcript variant 2 (SIAT4A)[a]	BC018357	1	Promoter	compatible
Homo sapiens protein tyrosine phosphatase, receptor type, N polypeptide 2	BC034040	1	3′ region	N.D.
Homo sapiens prostaglandin E2 receptor	L25124	1	Promoter	N.D.
Homo sapiens polyamine modulated factor-1	AF141310	1	3′ region	N.D.
Homo sapiens nuclear receptor subfamily 5, group A, member 1	BC032501	1	3′ region	N.D.
Homo sapiens NEL-like 2 (NELL2)[a]	BC020544	1	Promoter	compatible
Homo sapiens mRNA; cDNA DKFZp667I0324	AL832828	1	N.D.	N.D.
Homo sapiens mRNA; cDNA DKFZp564L0472	AL080101	1	3′ region	N.D.
Homo sapiens mRNA; cDNA DKFZp564G1482	AL136698	1	Promoter	N.D.
Homo sapiens mRNA, chromosome 1 specific transcript KIAA0495	AB007964	1	Promoter	N.D.
Homo sapiens chromosome 13 open reading frame 21 (C13orf21)[a]	BC029067	1	Promoter	compatible
Homo sapiens mRNA for SOX7 protein[a]	AJ409320	1	Promoter	compatible
Homo sapiens mRNA for nephrosis 2, idiopathic, steroid-resistant (NPHS2)[a]	AJ279254	1	Promoter	compatible
Homo sapiens mRNA for MDC2 alpha, MDC2 beta	AB009671	1	Promoter	N.D.
Homo sapiens mRNA for KIAA0641 protein	AB014541	1	N.D.	N.D.

Table II. *Continued*

Gene	GenBank accession no.	No. of MCA–RDA clones	Position of MCA–RDA clones	COBRA data
Homo sapiens mRNA for transcription factor 7-like 1 (TCF7L1)[a]	AB031046	1	Promoter	compatible
Homo sapiens mRNA for calmegin (CLGN)[a]	D86322	1	Promoter	compatible
Homo sapiens mRNA for ADAMTS19 protein[a]	AJ311904	1	Promoter	compatible
Homo sapiens microtubule-associated protein 1B, transcript variant 1	NM_005909	1	Promoter	N.D.
Homo sapiens matrix metalloproteinase-21	AF520613	1	Exon 2	N.D.
Homo sapiens KIAA0534 protein	BC047716	1	Promoter	N.D.
Homo sapiens hypothetical protein MGC49007	BC041175	1	N.D.	N.D.
Homo sapiens hypothetical protein LOC284801	BC036201	1	Promoter	N.D.
Homo sapiens hypothetical protein LOC283887[a]	BC023651	1	Promoter	compatible
Homo sapiens hypothetical protein BC009980	BC009980	1	Promoter	N.D.
Homo sapiens GATA binding protein 2	BC051342	1	Promoter	not compatible
Homo sapiens forkhead-related transcription factor FREAC-9	AF042832	1	Exon 1	N.D.
Homo sapiens erythroblast macrophage protein EMP	AF084928	1	Promoter	N.D.
Homo sapiens Enah/Vasp-like (EVL)[a]	BC023997	1	Promoter	compatible
Homo sapiens cytokine receptor-like factor 1	BC044634	1	Promoter	N.D.
Homo sapiens cystathionine beta-synthase (CBS)[a]	L14577	1	Promoter	compatible
Homo sapiens clone DNA68818 PSST739	AY358393	1	Promoter	N.D.
Homo sapiens ceh-10 homeodomain containing protein	AY336059	1	Exon 1	N.D.
Homo sapiens cDNA FLJ42875	AK124865	1	Promoter	N.D.
Homo sapiens cDNA FLJ41549[a]	AK123543	1	Promoter	compatible
Homo sapiens cDNA FLJ38293	AK095612	1	Promoter	N.D.
Homo sapiens cDNA FLJ37464[a]	AK094783	1	Promoter	compatible
Homo sapiens cDNA FLJ33739	AK091058	1	3′ region	N.D.
Homo sapiens cDNA FLJ14238	AK024300	1	Promoter	N.D.
Homo sapiens cDNA clone IMAGE:6025756	BC064906	1	Promoter	N.D.
Homo sapiens bridging integrator protein-1	U68485	1	3′ region	N.D.
Homo sapiens brain tumor associated protein LRRC4[a]	AF196976	1	Promoter	compatible
Homo sapiens apoptosis-associated tyrosine kinase, mRNA	BC047378	1	3′ region	N.D.
ho64c01.x1 Soares_NFL_T_GBC_S1 *Homo sapiens* cDNA clone	AW873619	1	Promoter	N.D.
Helix pomatia sulfatase 1 precursor	AF109924	1	Promoter	N.D.
H.sapiens mitogen inducible gene mig-2 (MIG2)[a]	Z24725	1	Promoter	compatible
GENCOURT_8532095 NIH_MGC_113 *Homo sapiens* cDNA clone	BU899260	1	N.D.	N.D.
EST379664 MAGE resequences, MAGJ *Homo sapiens* cDNA	AW967589	1	N.D.	N.D.
BX394700 *Homo sapiens* NEUROBLASTOMA COT 25-NORMALIZED	BX394700	1	Promoter	N.D.
AL545903 *Homo sapiens* PLACENTA COT 25-NORMALIZED	AL545903	1	Promoter	N.D.
AGENCOURT_8219616 Lupski_sympathetic_trunk *Homo sapiens* cDNA clone	BQ722471	1	N.D.	N.D.
AGENCOURT_7546470 NIH_MGC_70 *Homo sapiens* cDNA clone	BQ218409	1	Promoter	N.D.
7k34e06.x1 NCI_CGAP_Ov18 *Homo sapiens* cDNA clone IMAGE:3477227	BF058764	1	N.D.	N.D.
602695383F1 NIH_MGC_97 *Homo sapiens* cDNA clone IMAGE:4827284	BG722892	1	N.D.	N.D.
Homo sapiens mRNA for KIAA0711 protein	AB018254	1	3′ region	N.D.
Homo sapiens E2F binding protein	AY152547	1	Exon 1	N.D.
Homo sapiens cDNA FLJ38336	AK095655	1	3′ region	N.D.

N.D., not determined. COBRA data indicated that methylation level of the MCA–RDA clones in CRCs positive for *MLH1* methylation was increased (compatible) or not (not compatible) compared with that in CRCs negative for *MLH1* methylation.
[a]Clones analyzed in a test set of samples.

By using COBRA, their CpG methylation status was assessed among the samples used in MCR–RDA. As indicated in Table II, 28 fragments out of 35 were preferentially methylated in the tester DNA, while 7 of them were not.

The methylation status of such 28 fragments was further tested in clinical specimens that had not been used for the initial screening. This test set included eight cancer specimens positive for *MLH1* methylation and the paired normal colon tissue as well as eight cancer specimens negative for *MLH1* methylation (Table I).

The methylation status of each genomic fragment in the clinical specimens is shown color-coded in Figure 1; fragments with a methylation level of $\geq 10\%$ as determined by COBRA are indicated in red, whereas those with a methylation level of $< 10\%$ are shown in blue. Most genomic fragments were extensively methylated in most or all of the cancer specimens positive for *MLH1* methylation, but not in those negative for *MLH1* methylation. The difference in CpG methylation for the MCA–RDA products between the methylated and unmethylated groups of patients was thus confirmed in a distinct test set of CRC specimens.

A more detailed inspection of the data in Figure 1, however, indicates that the MCA–RDA products can be separated into three subgroups on the basis of their methylation profiles. The genomic fragments in the first group (*MIG2* to *NPHS2* in Figure 1) were also methylated in $\geq 25\%$ of the paired normal colon tissue samples. The fragment corresponding to *MIG2*, for instance, was methylated in all of the *MLH1* methylation-positive cancer specimens and the respective normal tissue. Methylation of these genomic regions thus probably occurred in each patient before the development of CRC and might be related to the aging process.

The genomic fragments in the second group (*BMP3* to *DPYSL3*) were not methylated in normal colon tissue but were methylated in $\geq 25\%$ of cancer specimens that were negative for *MLH1* methylation. The methylation of these